Cannabidiol reverses neuroimmune priming and microglial exhaustion in aged Gulf War Illness mice

Kwang-Mook Jung

kmjung@uci.edu

University of California, Irvine https://orcid.org/0000-0003-4096-6953

Hye-Lim Lee

University of California Irvine

Heidi Avalos

University of California, Irvine

Joelle Hong

University of California, Irvine

Erica Squire

University of California, Irvine https://orcid.org/0000-0003-2833-3379

Daniele Piomelli

University of California, Irvine

Article

Keywords:

Posted Date: July 3rd, 2026

DOI: https://doi.org/10.21203/rs.3.rs-10072088/v1

Additional Declarations: There is **NO** Competing Interest.

Cannabidiol reverses neuroimmune priming and microglial exhaustion in aged Gulf War Illness mice

Hye-Lim Lee[1]*, Heidi C. Avalos[1]*, Joelle Hong[1], Erica Squire[1], Daniele Piomelli[1], and Kwang-Mook Jung[1,#]

[1] Department of Anatomy and Neurobiology, University of California, Irvine, CA, 92697, USA.

* Equal contribution.

[#]**Corresponding author:**

Kwang-Mook Jung, Ph.D.

Department of Anatomy and Neurobiology, 3105 Gillespie Neuroscience Research Facility, University of California Irvine, CA, 92697-1275, USA

kmjung@uci.edu

Word counts: title 13; abstract 147; main text 4,356; methods 977. Display items: 5 figures. References: 48.

Abstract

Gulf War Illness (GWI) affects up to one-third of 1990–1991 Gulf War veterans and is associated with chronic low-grade neuroinflammation, yet its cellular substrates remain unclear and targeted pharmacological therapies are still limited. By integrating hippocampal single-nucleus RNA sequencing (snRNA-seq) with bulk RNA-seq analyses of whole-brain and FACS-purified microglia in an established GWI mouse model, we uncovered a multi-lineage primed neuroimmune signature in aged GWI mice. Systemic lipopolysaccharide (LPS) elicited an amplified pro-inflammatory response in the brains of GWI mice compared to age-matched controls, yet paradoxically, microglia were transcriptionally hyporesponsive to LPS, with inverted antigen presentation module score indicative of a microglial exhaustion phenotype. Chronic cannabidiol (CBD) attenuated neuroimmune priming at baseline, reshaping microglial translational and energetic states. Under immune-stimulated conditions, CBD suppressed the parenchymal hyper-response and partially restored GWI-associated deficits in microglial antigen presentation and oxidative phosphorylation, defining a therapeutic axis amenable to pharmacological intervention.

Introduction

Gulf War Illness (GWI) is a chronic multi-symptom disorder affecting an estimated 25–32% of the approximately 700,000 veterans of the 1990–1991 Persian Gulf War. It is characterized by persistent cognitive impairment, fatigue, pain, and mood dysregulation that have remained unresolved for more than three decades[1-6]. Neurologic and neuropsychiatric manifestations are among the most prominent concerns, encompassing difficulties with memory encoding and retrieval, sustained attention, mood regulation, and the attainment of restorative sleep. The etiology of GWI is widely attributed to wartime co-exposure to a constellation of neurotoxicants, including the acetylcholinesterase inhibitor and nerve-agent prophylactic pyridostigmine bromide (PB), the pyrethroid insecticide permethrin (PER), the repellant DEET, and organophosphate nerve agents, compounded by physiological stress[7-9].

Persistent neuroinflammation has emerged as the central mechanistic driver of GWI-associated brain dysfunction. The neuroimmune hypothesis of GWI holds that chronic elevation of cytokines and reactive oxygen species in the brain, persisting long after the initial instigating exposures, drives the associated neuropathology and behavioral deficits[10-13]. This was clinically demonstrated in a positron emission tomography (PET) study using the translocator protein (TSPO) ligand [^{11}C]PBR28, which provided the first *in vivo* imaging evidence of widespread neuroinflammation in veterans diagnosed with GWI[14]. At the molecular level, chronic neuroinflammation in rodent GWI models is characterized by persistent proinflammatory microglia with NLRP3 inflammasome activation, astrocyte hypertrophy, and elevated hippocampal and cortical concentrations of 5-lipoxygenase and its product, cysteinyl leukotrienes and leukotriene B_4[7]. Extracellular HMGB1, leaked from injured neurons, acts as a sustained paracrine alarmin that drives microglial activation and complement pathway induction, linking acute toxic injury to the self-sustaining neuroinflammatory loop observed at protracted timepoints in animal models[15]. These central inflammatory signals are amplified in GWI veterans, whose circulating cytokine

profiles and transcriptional signatures resemble those of autoimmune disorders and who show elevated serum HMGB1 capable of priming microglial reactivity *ex vivo*[16].

Critically, the neuroinflammatory substrate of GWI does not remain static over time but interacts with the biology of aging to progressively worsen cognitive outcomes. Approximately 12% of a middle-aged cohort of Gulf War veterans (median age 52) met diagnostic criteria for mild cognitive impairment (MCI) — a syndrome typically prevalent only in adults aged 70 years or older — implying substantial premature neurocognitive aging[17,18]. Longitudinal MRI in established GWI mouse models corroborates this observation, demonstrating markedly earlier reductions in total brain volume indicative of accelerated brain aging, consistent with clinical evidence that veterans with more severe GWI symptoms are disproportionately affected by age-related cognitive decline [19]. Organophosphate exposure during the Gulf War also has been linked to this trajectory through induction of a senescence-associated secretory phenotype (SASP), a pro-inflammatory secretome that propagates tissue dysfunction and accelerates biological aging [20,21].

As the resident immune cells in brain parenchyma, microglia are the principal cellular interface through which aging and neuroinflammation converge. Research indicates that GWI-related toxic exposures induce a chronically primed microglial state that yields exacerbated responses to subsequent inflammatory challenges, consistent with a two-hit model in which initial chemical insults sensitize microglia to amplified reactivity upon later stressors, including aging itself [22,23]. Using a GWI mouse model, we recently identified a paradoxical functional dissociation in microglia: GWI microglia exhibit sustained suppression of sensome and surveillance genes and a globally blunted transcriptional response to lipopolysaccharide (LPS), yet show heightened AP-1–driven induction of the pro-inflammatory cytokines *Il1b* and *Tnf* following immune stimulation[24]. This combination of impaired surveillance capacity and sensitized pro-inflammatory signaling may foster the emergence of hyperreactive, exhaustion-like microglia

over time as they interact with aging-associated changes in the brain, a trajectory that remains to be systemically elucidated[25].

These microglial abnormalities were mechanistically linked to disruption of the endocannabinoid (ECB) system, an endogenous signaling network that constrains neuroinflammation via cannabinoid receptor activation on microglia and other brain cells. In our prior work, GWI mice exhibited reduced brain levels of the ECB agonist anandamide (AEA), accompanied by elevated transcription of fatty acid amide hydrolase (FAAH), the primary catabolic enzyme for AEA. Pharmacological FAAH inhibition restored AEA tone and corrected anxiety-, depression-, and extinction-related behavioral deficits in the GWI model[24]. Because the non-intoxicating phytocannabinoid cannabidiol (CBD) can enhance ECB tone and exert broad anti-neuroinflammatory effects[26,27], it represents a translationally attractive strategy for engaging this same axis. Furthermore, CBD has been recently shown to effectively alleviate cognitive and mood impairments as well as hyperalgesia in a rat model of GWI[28].

Here we applied a multi-resolution transcriptomic strategy in an aged GWI mouse model, combining hippocampal single-nucleus RNA sequencing (snRNA-seq), whole-brain bulk RNA-seq under basal and LPS-challenged conditions, and bulk RNA-seq of FACS-purified microglia from the same experimental design. We further evaluated chronic CBD as a candidate intervention. The integrated analysis revealed a dual brain-hyperresponsive and microglia-exhausted phenotype as the cellular substrate of aged GWI and identified a pharmacologically tractable, ECB-based therapeutic axis engaged by chronic CBD treatment.

Results

A multi-lineage primed neuroimmune state in the aged GWI hippocampus

To map disease-associated alterations of the cellular and molecular landscape in the hippocampus of aged GWI mice, we performed comparative snRNA-seq profiling of whole hippocampus from GWI and control (Ctrl) groups (**Fig. 1a**). A single library per group was generated from pooled hippocampal tissue of n = 3 biological replicates, and downstream analyses were accordingly focused on aggregated gene-level signals. After quality control, 37,745 high-quality nuclei (19,115 from Ctrl and 18,630 from GWI) were retained, Harmony-integrated, and annotated into nine broad lineages and 24 fine cell-type subtypes (**Fig. 1b-1d**, **Supplementary Fig. S1, S2**, and **Supplementary Table S1**). Cellular composition was broadly preserved with selective shifts: at the broad lineage level, excitatory neurons decreased 9.8% in GWI, oligodendrocyte precursor cells (OPCs) expanded 56.7%, and microglia contracted 8.1% (**Fig. 1e**); at the fine level, the excitatory loss was driven by dentate granule cell subtypes (ExN-DG-Zic1, −55.8%; ExN-DG-Drd1, −34.0%; and ExN-DG-Drd2, −29.2%) and the subicular ExN-Sub-Foxp2 population (−32.0%) (**Supplementary Table S1**). Cell type-specific comparative analysis using GSEA on the broad cell types followed by GO:BP, KEGG, and Hallmark enrichment analyses revealed a multi-lineage signature in aged GWI hippocampus with major alterations in microglia, inhibitory neurons, and excitatory neurons (**Fig. 1f** and **Supplementary Table S2**). In particular, GSEA-GO:BP and -Hallmark analyses on the broad-lineage cell type clusters dataset found that microglia exhibit a chronically immune-activated, ‘primed’ transcriptional state, with upregulated genes significantly enriched for activation of immune response (normalized enrichment score (NES) = +1.74, Padj = 0.041), leukocyte-related processes, and endocytosis (**Fig. 2a** and **Supplementary Fig. S3**). A similar enrichment was also observed in the fine cell type analysis, which localized the strongest immune-priming signal to the homeostatic microglia cluster (Micro-Homeo), in which both GSEA-GO:BP and Hallmark

reached statistical significance for positive regulation of immune response, complement, and Il6-Jak-Stat3 signaling (**Fig. 2b** and **Supplementary Fig. S4**) with leading-edge contributions from *C1qa, C1qb, C1qc, Stat3,* and *Il6st* (**Fig. 2c**). Given that immune activation in microglia is coupled to a shift toward aerobic glycolysis[29], we next examined glycolytic gene expression across the broad microglial cluster and its fine subsets (**Supplementary Fig. S5**). The glycolytic shift was concentrated in the activated microglia subset (Micro-Act), recapitulating the canonical mouse glycolytic-activation signature[29,30]: the most strongly upregulated genes were *Ldha* (+0.26), *Pgk1* (+0.28), and *Hk2* (+0.24), with *Eno1* (+0.13) and *Gapdh* (+0.11). By contrast, the homeostatic and broad microglial populations remained flat-to-negative across glycolytic enzymes, suggesting that the two fine microglia subsets capture distinct, complementary facets of the microglial response to chronic GWI pathology. OPCs were engaged in regeneration (NES = +1.80, Padj = 0.028) and cell adhesion, suggesting ongoing or attempted repair (**Fig. 2d** and **Supplementary Fig. S3**), and inhibitory neurons showed altered transcriptional programs (negative regulation of transcription by RNA polymerase II, NES = −1.95, Padj = 0.038), consistent with disturbed homeostasis and potential network-level dysfunction (**Fig. 2e** and **Supplementary Fig. S3**).

Cell type-specific module score analysis across 39 functional modules (12 pan and 27 cell type-specific) in the 8 broad cell lineages confirmed similar multi-lineage primed neuroimmune signature in GWI hippocampus (**Fig. 2f** and **Supplementary Table S3**). Microglia showed coordinated up-regulation across the innate immune panels (Phagocytosis_Lysosome module, Δ GWI-Ctrl = +1.27; Pan_Chemokine, +1.13; Pan_Complement, +0.63; and Lipid_DAM, +0.44). OPCs were primed by cytokine and interferon signaling (Pan_Complement, +0.79; Pan_Cytokine, +0.64; and Pan_Interferon_Response, +0.71), astrocytes exhibited an A1-leaning polarization (A1_Neurotoxic, +0.42; and A2_Neuroprotective, −0.71), inhibitory neurons showed elevated Pan_Chemokine, Pan_Interferon_Response, and Pan_Oxidative_Stress scores (Δ = +0.85 to

+1.13), and endothelium engaged BBB_Tight_Junction (+0.79) and Pan_Interferon_Response (+0.71) signatures (**Fig. 2f**).

Systemic LPS triggers an amplified brain-wide neuroinflammatory response in aged GWI mice

To investigate the functional consequences of the chronically immune-activated state, we performed whole-brain bulk RNA-seq on aged Ctrl and GWI mice under systemic LPS (0.33 mg/kg)-challenged and basal (PBS-injected) conditions (**Supplementary Table S4**). Principal component analysis (PCA) separated GWI samples from control in both basal and LPS-stimulated conditions (**Fig. 3a** and **3b**). Consistent with the snRNA-seq findings, the unchallenged GWI brain showed subtle transcriptional alterations (no DEGs at Padj < 0.05; 365 DEGs at relaxed P < 0.05 and $|\log_2 FC| > 0.5$) (**Supplementary Table S4**), but pre-ranked GSEA revealed a signature of elevated cytoplasmic translation and ribosome programs (GO:BP cytoplasmic translation, NES = +2.11, Padj = 3.90e-06; KEGG ribosome, NES = +2.68, Padj = 3.49e-08) and reduced mRNA processing/catabolism (**Fig. 3c, Supplementary Fig. S6a**).

LPS elicited the canonical neuroinflammatory program in both GWI and control mice (**Supplementary Fig. S7**), but the magnitude was strikingly greater in GWI. In control brains, LPS induced 59 significant DEGs (52 up, 7 down at Padj < 0.05, $|\log_2 FC| > 0.5$) and 116 up-regulated GO:BP terms (**Fig. 3d** and **Supplementary Table S4**), led by synapse pruning (Padj = 4.98e-06), microglial cell activation, and macrophage activation (**Supplementary Table S5**). In GWI brains, the same challenge produced 143 DEGs (132 up, 11 down) and 620 up-regulated GO:BP terms — a 2.4- and 5.3-fold increase, respectively (**Fig. 3d** and **Supplementary Table S4**). Top GO terms in GWI mice after LPS reached enrichment significances orders of magnitude beyond control mice (leukocyte-mediated immunity, Padj = 2.71e-23; cell killing, Padj = 3.92e-15; phagocytosis, Padj = 1.02e-13; and positive regulation of cytokine production, Padj = 1.97e-10) (**Supplementary Table S5**), and core inflammatory mediators such as *C1qa/b/c, Ly6a, Ly6c1,*

Cx3cr1, Fcgr3, and *Tyrobp* populated the leading edges of multiple gene sets (**Supplementary Fig. S7c**). Direct comparison between GWI and control brains after LPS confirmed a clearly higher pro-inflammatory status in GWI, including significant enrichment to leukocyte-mediated immunity, positive regulation of innate immune response (GSEA-GO) and leukocyte trans-endothelial migration (GSEA-KEGG) (**Fig. 3e** and **Supplementary Fig. S6b**) with strong increases of T-cell-related (*Ctram, Il16, Il22*, and *Ptpn22*), astrocyte-related (*A2m, Sox9*, and *Trpv4*), and mitochondrial (*mt-Nd5* and *mt-Nd6*) transcripts (**Fig. 3f**). An unexpected reduction in ribosomes was identified in GSEA-KEGG analysis (NES = -2.05, Padj = 7.07e-06) (**Supplementary Fig. S6b**).

In addition, the formal GWI × LPS interaction (ΔLPS) analysis isolated a GWI-specific phenotype that was not merely an enlarged control response (**Fig. 3g** and **3h**). On the GWI-amplified positive side, GSEA was enriched for leukocyte-mediated immunity (NES = +1.79, Padj = 1.84e-04), regulation of innate immune response (NES = +1.72, Padj = 1.84e-04), and leukocyte transendothelial migration (KEGG NES = +1.95, Padj = 0.001), with leading-edge genes spanning T-cell co-stimulation and adhesion (*Icosl, Crtam, Cd86, Itgal, Itgb2, Cldn5, Ocln, Pecam1*), innate sensing (*Tlr3/4/7, Nlrp3, Il1r1, Casp4*), and microglial activation (*Tyrobp, Ptprc, Fcgr1–4, Btk*) (**Fig. 3g, 3h, Supplementary Figure S6c,** and **Supplementary Table S6**). On the GWI-amplified negative side, the interaction revealed pronounced suppression of synaptic and translational machinery: translation at synapse/presynapse/postsynapse (GO-BP NES ≈ −2.8; Padj ≤ 2.03e-07), cytoplasmic translation (NES = −2.12, Padj = 6.89e-07), regulation of synapse organization, dendrite development, and KEGG oxidative phosphorylation (NES = −1.75, Padj = 0.002) (**Fig. 3g, 3h, Supplementary Figure S6c,** and **Supplementary Table S6**). The GWI brain therefore mounts an exaggerated vascular/leukocyte-engagement response coupled to deeper repression of synaptic-translation and neuronal-activity programs compared to controls.

FACS-purified GWI microglia mount a blunted LPS response defining a microglial exhaustion phenotype

To determine whether the amplified parenchymal LPS response is driven by aberrant activation of GWI microglia, we carried out comparative transcriptome analysis of FACS-purified (CD45mid /CD11b^{+}/CD11a^{-}) microglia from the brain of GWI and control mice (**Fig. 4a, 4b,** and **Supplementary Fig. S8**). At baseline, GWI microglia produced no FDR-significant DEGs vs control at Padj < 0.05, $|\log_2 FC| > 0.5$ (**Supplementary Table S7**), but exhibited a positive GSEA signature for translation (GO:BP translation at synapse, NES ≈ +2.9, Padj = 8.06e-08), ribosome, and oxidative phosphorylation (KEGG ribosome, NES = +3.30, Padj = 1.17e-08; KEGG oxidative phosphorylation, NES = +2.77, Padj = 1.17e-08), consistent with a primed basal state (**Fig. 4c** and **Supplementary Fig. S8a**).

Under LPS challenge, however, GWI microglia were strikingly hyporesponsive. Control microglia produced 2,768 significant DEGs (1,391 up, 1,377 down) at Padj < 0.05, $|\log_2 FC| > 0.5$, and 445 enriched GO:BP terms (**Fig. 4d, Supplementary Table S7,** and **Supplementary Figure S9**), led by the canonical microglial-activation program (ribosome biogenesis, Padj = 1.64e-36; rRNA processing, Padj = 2.22e-25; cytoplasmic translation, Padj = 6.84e-17) (**Supplementary Table S8**), with the classical homeostatic-to-activated module shift (Homeostatic, Δ = −1.81; Complement, +1.36; Interferon_Antiviral +1.74, Phagocytosis_Lysosome +0.87; all Padj < 0.05) (**Fig. 4e**). In contrast, GWI microglia produced only 1,427 DEGs (685 up, 742 down) and 82 enriched GO terms under the same statistics power (**Fig. 4d, Supplementary Table S7,** and **Supplementary Figure S9**), with ribosome biogenesis (Padj = 2.14e-23) displaying a > 12-log-unit attenuation compared to control microglia (**Supplementary Table S8**). None of the canonical activation module shifts reached significance in GWI microglia, and two modules inverted: Antigen_Presentation Δ = −1.46 (Padj = 0.011) and Lipid_DAM Δ = −1.31 (Padj = 0.028) (**Fig. 4e**), indicating that GWI microglia decreased their antigen presentation and disease-associated

microglia (DAM)-like transcriptional programs upon LPS challenge — the inverse of the control response. Interestingly, direct comparison between GWI and control microglia after LPS using GSEA-GO:BP analysis found a significant enrichment with negative NES to the GO terms for proton motive force-driven ATP synthesis, mitochondrial translation, ATP biosynthetic process, and oxidative phosphorylation (NES = −2.89, −2.83, −2.69, and −2.67, respectively; all Padj = 1.7e-08) (**Fig. 4f**) with reductions in the *Rpl, Nduf, Atp5/6, Cox*, and *mt-Nd* family genes (**Fig. 4g**), suggesting that GWI microglia respond to immune challenge with impaired metabolic flexibility and may not be sufficiently meeting energetic demands.

The formal GWI × LPS interaction analysis recovered the same dissociation in GWI microglia (KEGG ribosome, NES = −3.70, Padj = 2.93e-09; KEGG oxidative phosphorylation, NES = −3.36, Padj = 2.93e-09; KEGG antigen processing and presentation, NES ≈ −2.85, Padj = 2.93e-09; GO:BP translation at synapse, NES = −3.24, Padj = 1.52e-08;) (**Fig. 4h, Supplementary Fig. S8c**), with leading edges spanning ribosomal proteins, MHC-I/II loci (*H2-D1, H2-K1, H2-DMa, H2-DMb1/2, B2m, Tap1, Tapbp*), and interferon-stimulated genes (*Ifit1/3, Mx1/2, Oas1a/g, Isg15, Irf7, Irf9*) (**Fig. 4i**).

The juxtaposition of a hyperresponsive brain tissue and a hyporesponsive microglial compartment defines a brain-microglia dissociation paradox proposing that the parenchymal neuroinflammation might be driven predominantly by non-microglial cells such as astrocytes, endothelium, and infiltrating leukocytes (**Fig. 3e** and **3g**), while microglia fail to mount a competent immune activation response. We interpret this signature as a microglial-exhaustion phenotype reflecting the convergence of aging, chronic GWI-associated priming, and the acute LPS challenge.

Chronic CBD partially rescues both arms of the dissociation phenotype of GWI brain

To examine the effects of CBD on GWI-associated transcriptional deficits in the brain, we treated GWI mice with CBD (30 mg/kg, i.p.) once daily for 28 days, followed by a 2-week maintenance

phase at the same dose administered once every 2 days; vehicle-arm animals received an equal volume of vehicle. Then, mice were subjected to an immune challenge with LPS (0.33 mg/kg, i.p.) and sacrificed 24 hours later for brain tissue collection (**Fig. 5a**). At baseline, although CBD produced no FDR-significant DEGs in GWI mice at Padj < 0.05 (**Supplementary Table S4** and **Supplementary Fig. S10**), pre-ranked GSEA revealed a coherent and statistically significant suppression of the constitutive ribosome and oxidative phosphorylation programs that defines the primed state of GWI brain (GO:BP translation at pre-/post-/synapse, NES ≤ −2.89; GO:BP ATP synthesis coupled electron transport, NES = −2.72, Padj ≤ 2.8e-08; KEGG Ribosome, NES ≤ −2.29; KEGG oxidative phosphorylation, NES ≤ −2.29; Padj ≤ 2.5e-05; **Fig. 5b, Supplementary Fig. S10c**). CBD therefore may act at immune baseline by attenuating chronic priming. After LPS, CBD strongly attenuated the GWI-amplified parenchymal neuroinflammatory program. Whole-brain bulk RNA-seq identified 36 significant DEGs at Padj < 0.05, $|\log_2 FC| > 0.5$ (0 up, 36 down) (**Supplementary Table S4**) and 173 down-regulated GO:BP plus 28 down-regulated KEGG terms, led by leukocyte-mediated immunity (Padj = 7.56e-08) and lymphocyte-mediated immunity (Padj = 7.56e-08) — the inverse of the LPS-amplified GWI signature (**Supplementary Table S9**). GSEA-GO:BP analysis confirmed that CBD significantly dampens pro-inflammatory response to LPS in GWI brain, identifying a reduction in antigen processing and presentation of peptide antigen and leukocyte-mediated immunity (NES ≤ −2.63) (**Fig. 5c**).

In FACS-purified microglia from the LPS group, CBD produced 344 significant DEGs at Padj < 0.05, $|\log_2 FC| > 0.5$ (167 up, 177 down) (**Supplementary Table S7** and **Supplementary Fig. S11**) and exhibited a distinct pattern: no upregulated GO:BP terms were identified, whereas 51 down-regulated GO:BP terms were dominated by ribosome biogenesis (Padj = 2.24e-5), indicating that CBD does not reverse the most deeply suppressed axis of microglial exhaustion (**Supplementary Table S10**). However, under a more relaxed threshold (P < 0.05 and $|\log_2 FC| >$ 0.5), 934 up-regulated DEGs and 136 GO:BP terms were identified, dominated by mitotic and

chromosome-segregation pathways (chromosome segregation, Padj = 4.04e-18) (**Supplementary Tables S7** and **S10**). GSEA-GO:BP analysis confirmed these findings, revealing a significantly elevated mitotic cell cycle process (NES = 2.26) and reduced ribosome biogenesis (NES = -3.19) (**Fig. 5d**)**.** Critically, however, directed functional module scoring showed selective rescue of microglial competence: Antigen_Presentation Δ = +0.65 (Padj = 0.029), partially reversing the GWI-induced suppression of Δ = −0.89 (**Fig. 5e**). The formal CBD × LPS interaction within microglia confirmed a partial-rescue profile dominated by elevated mitochondrial energy metabolism (GSEA-GO:BP proton motive force-driven ATP synthesis, NES = +3.20, Padj = 2.09e-08; GSEA-KEGG oxidative phosphorylation, NES = +3.17, Padj = 3.19e-09) (**Fig. 5f, Supplementary Table S11**) and a notable up-regulation of GSEA-KEGG ribosome (NES = +3.03, Padj = 3.19e-09) driven by *Rpl/Rps/Mrpl/Mrps* gene families, alongside concurrent down-regulation of GSEA-GO:BP ribosome biogenesis (NES = −2.67, Padj = 2.09e-08) driven by upstream regulators (*Nmd3, Surf6, Usp16, Ddx51, Gtpbp4*)(**Fig. 5g, Supplementary Table S11**). Finally, CBD treatment was associated with significant reductions in *Cnr2,* which encodes cannabinoid CB2 receptors, in LPS-stimulated GWI mice in both whole brain and purified microglia (Log_2[CBD/Veh] = -1.17, P = 0.046; and Log_2[CBD/Veh] = -0.63, P = 0.031, respectively) (**Supplementary Fig. S12**).

Therefore, these results indicate that CBD restores antigen presentation, oxidative metabolism, and structural ribosomal proteins while leaving regulators of ribosome biogenesis depressed in immune-stimulated GWI microglia.

Discussion

By integrating snRNA-seq, whole-brain bulk RNA-seq, and bulk RNA-seq of FACS-purified microglia from a model of GWI in aged mice under matched basal and LPS-challenged conditions, we identify a coherent dual transcriptional phenotype that defines the cellular substrate of aged GWI: a system-wide, low-amplitude priming of innate-immune and cellular-stress programs that becomes physiologically consequential under acute immune challenge, paradoxically coupled to a microglial compartment that is transcriptionally exhausted and unable to mount a competent activation program. The snRNA-seq atlas localizes the primed state across multiple lineages — microglia (complement, phagocytic/lysosomal, lipid-DAM), OPCs (IL-6/STAT3, interferon, UPR), astrocytes (A1-leaning polarization), and inhibitory neurons (interferon, chemokine, oxidative stress) — and is corroborated at the bulk-tissue level, providing cross-platform support for the chronic-pro-inflammation hypothesis of GWI derived from cytokine, neuroimaging, and post-mortem evidence in veterans[10-14]. Notably, the immune-priming transcriptional signal and the glycolytic metabolic shift localized to different fine subsets—priming to Micro-Homeo and glycolysis to Micro-Act—indicating that the two subsets capture distinct, complementary facets of the microglial response to chronic GWI pathology. This dissociation aligns with the established microglial priming, or "two-hit," framework, in which an initial insult sensitizes microglia to a poised state — not elevated at baseline but predisposed to an exaggerated response upon secondary challenge — without itself constituting overt activation[23]. Our data extend this framework metabolically: whereas the immune-priming transcriptional signature localized to the homeostatic subset (Micro-Homeo), the glycolytic Warburg-like shift was confined to the activated subset (Micro-Act), suggesting that metabolic reprogramming is a feature of committed activation rather than the primed state itself.

The most surprising finding is the dissociation between the brain-wide versus the microglia-intrinsic responses to LPS. Whole-brain bulk RNA-seq revealed a 2.4-fold larger DEG response

and 5.3-fold more enriched GO:BP terms in GWI versus control brains, with a GWI-specific axis of vascular/BBB leukocyte engagement coupled to deeper synaptic-translation suppression. In striking contrast, FACS-purified microglia from the same animals were transcriptionally hyporesponsive, with the canonical microglial-activation module shifts absent in GWI and two activation modules (Antigen_Presentation, Lipid_DAM) moving in the wrong direction. This juxtaposition — to our knowledge, an unexpected configuration in neuroinflammation models — implies that the parenchymal neuroinflammation is driven predominantly by non-microglial compartments such as astrocytes, endothelium, infiltrating leukocytes, or neurons themselves, while microglia fail to provide the resolution functions including phagocytic clearance, antigen handling, and interferon-mediated debris removal that normally terminate such responses[31-33]. The configuration provides a framework for the chronic neurocognitive features of GWI: persistent, inadequately resolved low-grade neuroinflammation coupled to suppression of synaptic-translation and neuronal-activity programs is mechanistically aligned with the cognitive, mood, and fatigue symptoms experienced by veterans[9,34] and with the treatment-refractoriness of those symptoms to broad anti-inflammatory monotherapies[35].

The microglial-exhaustion phenotype we describe extends a growing literature on microglial state biology beyond the canonical activation paradigm. Repeated peripheral LPS exposure in mice has been shown to induce durable innate immune memory in microglia that can manifest as either 'training' (amplified subsequent responses) or 'tolerance' (reduced responses), depending on prior exposure history[36]. CD22 has been identified as a checkpoint that actively restrains phagocytic and clearance functions in aged microglia[37], and age-related single-cell and transcriptomic studies have documented marked shifts in microglial state heterogeneity, including reduced activation capacity in subsets of aged microglia [38]. In human brains, 'dystrophic' microglia have been described in aging and in Alzheimer's disease, with morphological evidence of compromised function rather than overt pro-inflammatory activation[39,40]. Across multiple neurodegenerative

models, the DAM state [41], the Activated Response Microglia signature [42], and human single-cell atlases of Alzheimer's microglia[43] together demonstrate that microglial states are diverse, dynamic, and context-dependent. Our findings extend these frameworks in two specific ways. First, we describe a configuration in which primed and exhausted microglial states coexist — homeostatic microglia carry elevated complement and IL-6/JAK-STAT3 priming at baseline yet, under acute challenge, fail to deploy a canonical activation program and instead invert their antigen presentation and DAM-like modules. Second, the brain-vs-microglia dissociation localizes the parenchymal inflammatory response predominantly outside the microglial compartment, identifying non-microglial drivers as the immediate effectors that must be addressed therapeutically alongside microglial rescue. The configuration is mechanistically aligned with recent single-cell and biomarker work in post-acute SARS-CoV-2 (long COVID), which has similarly documented sustained parenchymal cytokine signatures alongside microglial reactivity and cognitive deficits[44,45].

In a rat model, CBD has been shown to effectively alleviate cognitive and mood impairments, as well as hyperalgesia, associated with chronic GWI[28]. In line with these findings, our results indicate that chronic CBD treatment normalizes both arms of the dual phenotype, and its mechanism of action is unlikely to reflect simple, acute immunosuppression. At baseline, pre-ranked GSEA reveals that CBD selectively attenuates the constitutive elevation of ribosome biogenesis and oxidative-phosphorylation programs that defines the primed GWI microglial ground state. Rather than being transcriptionally silent, CBD therefore acts at baseline by attenuating the chronic priming itself, reducing the constitutive metabolic and translational load on aged GWI microglia. Under LPS challenge, this anti-priming action translates into three coordinated rescues: (i) suppression of the GWI-amplified inflammatory response across 173 down-regulated GO:BP terms including leukocyte-mediated immunity; (ii) selective restoration of microglial competence functions — antigen presentation, oxidative phosphorylation, ATP

generation required for activation, and translation output via ribosomal-protein gene families — even though GO:BP ribosome biogenesis driven by upstream regulators remains down-regulated; (iii) induction of a microglial proliferation program, including chromosome segregation and mitotic nuclear division, consistent with cellular rejuvenation of the exhausted compartment and potentially the replacement of damaged microglia by newly generated cells. The therapeutic logic that emerges — pre-emption of chronic priming, rescue of energetic and translational capacity, and proliferation-driven rejuvenation — is mechanistically distinct from broad-spectrum anti-inflammatory drugs that blunt acute cytokine responses without restoring microglial function. These findings suggest that CBD may engage either directly or indirectly microglial ECB-related (e.g., CB_2, adenosine A_2A, TRPV1) and metabolic pathways to dampen pro-inflammatory signaling, reduce oxidative stress, and normalize mitochondrial respiration. By doing so, CBD may de-prime chronically sensitized microglia at baseline and, upon immune challenge, limits parenchymal hyperactivation while partially restoring deficits in antigen presentation and oxidative phosphorylation pathways.

Several limitations should frame interpretation. First, the snRNA-seq dataset uses a pooled-replicate design (one library per condition derived from three biological replicates per pool), which provides biological averaging at the input level but precludes formal between-sample statistical inference; accordingly, we prioritized gene-set-level analyses (module scoring and pre-ranked GSEA) and treated DEG calls as exploratory effect-size estimates, with key snRNA-seq findings independently corroborated in the bulk whole-brain and FACS-microglia experiments. Second, some bulk RNA-seq comparisons, particularly at basal, unstimulated conditions, are underpowered for Padj-significant gene-level calls and rely primarily on pathway-level GSEA. Third, our FACS strategy targets CD45mid/CD11b$^+$/CD11a$^-$ microglia and does not directly resolve border-associated macrophages or perivascular myeloid populations[46,47], which may contribute to the parenchymal response that microglia themselves do not mount. Finally, all data

are transcriptomic; functional validation of the microglial-exhaustion phenotype by phagocytosis, antigen presentation, and cytokine-release assays, together with direct quantification of brain-infiltrating leukocytes, represents an important next step to refine the mechanistic interpretation of the dissociation paradox and the CBD rescue.

Despite these constraints, the convergence of three independent transcriptomic modalities on a single coherent dual phenotype provides cross-platform support for the central finding, and the partial pharmacological rescue by chronic CBD indicates that both axes are biologically and therapeutically tractable. This framework of brain hyperresponsiveness coupled to microglial exhaustion may extend to other chronic conditions in which a primed parenchyma interacts with a compromised microglial compartment, including normal aging, post-acute sequelae of SARS-CoV-2 infection, and chronic stress states associated with occupational or environmental toxicant exposure.

Methods

Animals, GWI exposure paradigm, and experimental groups

Male C57BL/6J mice (19 months at endpoint) were used (Jackson Labs, Farmington, CT). All animals were housed in ventilated cages (4 per cage) with free access to chow and water in rooms maintained on a 12-h light/12-h dark cycle (lights on at 6:30 AM, off at 6:30 PM) with constant temperature (22±2°C) and humidity (55-60%). All procedures were approved by the Institutional Animal Care and Use Committee of the University of California, Irvine, and were carried out in strict accordance with the National Institutes of Health guidelines for care and use of experimental animals.

The GWI cohort was generated as described by Zakirova et al., using the combined Gulf War chemicals exposure protocol by administering 10 week-old mice with a 50 μL total volume of 0.7 mg/kg of pyridostigmine bromide and 200 mg/kg permethrin in 100% DMSO, or a 50 μL volume of vehicle via intraperitoneal injection (i.p.) daily, for 10 days [8]. Following exposure, animals were aged to 17.5 months and assigned to a 2 × 2 × 3 factorial design: Ctrl-Veh-PBS, Ctrl-Veh-LPS, GW-Veh-PBS, GW-Veh-LPS, GW-CBD-PBS, GW-CBD-LPS (n = 3–4 per condition for bulk RNA-seq; three pooled hippocampi per condition for snRNA-seq). CBD-arm animals received daily i.p. administration of CBD (30 mg/kg in 5% Tween 80/PBS) for 28 consecutive days, followed by maintenance dosing once every 2 days for an additional 2 weeks; vehicle-arm animals received an equal volume of vehicle. On the morning after the final dose, LPS-arm mice received a single intraperitoneal injection of 0.33 mg/kg LPS from *Escherichia coli* strain O111:B4 (L4130, Sigma Aldrich); PBS mice received an equal volume of sterile PBS. After 24 hours, mice were anesthetized with isoflurane (Pivotal veterinary, Loveland, CO), killed by decapitation, and the brains were removed.

Hippocampal nuclei isolation and snRNA-seq

Three hippocampi per condition (from three Control or GWI mice) were pooled and quickly frozen. They were processed as a single nuclei suspension per condition, yielding one sequencing library per group from three biological replicates. Single nuclei were isolated using a Miltenyi gentleMACS Dissociator (Miltenyi Biotec, Bergisch Gladbach, Germany), and suspensions were loaded onto a 10x Genomics Chromium Controller (Next GEM Single Cell 3' v3.1). Libraries were sequenced on an Illumina platform using paired-end 150 bp reads (PE150) to a depth of at least 25,000 reads per nucleus; all library preparation and sequencing were performed by Novogene (Beijing, People's Republic of China). Reads were aligned to the mouse reference genome (GRCm38/mm10) using Cell Ranger, and the resulting 10x HDF5 count matrices were imported into R for downstream analysis.

snRNA-seq processing and cell-type annotation

Analyses were performed in R 4.5.2 using Seurat v5.5.0. Nuclei were retained if 200 < nFeature_RNA < 6,000, nCount_RNA < 30,000, and percent.mt < 5%. Counts were log-normalized, 3,000 highly variable genes were selected, data were scaled regressing out percent.mt, and 50 principal components were computed. Harmony integration was applied across libraries, and clustering at resolution 0.4 yielded 33 clusters that were embedded by UMAP. Cluster annotation combined SingleR (MouseRNAseqData + ImmGenData) majority labels with canonical marker review and *FindAllMarkers* output, yielding 24 fine cell-type labels collapsed into nine broad lineages for primary inferential analyses.

Whole-brain bulk RNA-seq and FACS-purified microglia bulk RNA-seq

Total RNA was extracted from the whole brain using a Trizol/RNeasy hybrid method [24,48]. For microglia purification, quickly isolated brains were dissociated using the Adult Brain Dissociation kit (Miltenyi Biotec). Myelin was removed, and microglia were purified by flow cytometry cell sorting (FACS) as live CD45mid /CD11b^{+}/CD11a^{-} cells, as previously described [24,48]. Total RNA

was extracted, and samples with RNA integrity number ≥ 8.5 were used for RNA sequencing. RNAseq was conducted at Novogene (Bejing, People's Republic of China) using the Illumina NovaSeq platform with paired-end 150 bp (PE 150) sequencing strategy. Poly(A)-enriched stranded libraries were prepared and sequenced, and reads were aligned to GRCm38/mm10 to produce gene-level counts.

snRNA-seq differential expression, pathway enrichment, and module scoring

snRNA-seq transcriptional changes were assessed at all-nuclei, per-fine-celltype, and per-broad-lineage granularities using Wilcoxon rank-sum tests (*FindMarkers*, min.pct = 0.1, logfc.threshold = 0.1). Because the pooled-replicate design yielded one library per group, formal between-sample inference was not possible; nuclei were used as the analytic unit for these comparisons, framed as exploratory effect-size estimates (adjusted $P < 0.05$ and $|\log_2 FC| > 0.5$). Pre-ranked GSEA used clusterProfiler v4.18 against MSigDB Hallmark, GO:BP, and KEGG collections (msigdbr v26.1, species = mouse). snRNA-seq cell-type module scoring used the module panel described in **Supplementary Table S12**, with member-gene expression aggregated into per-(sample × broad-cell-type) pseudobulks, gene-wise z-scored across samples, and averaged.

Bulk RNA-seq differential expression, pathway enrichment, and module scoring

Whole-brain and FACS-microglia bulk datasets were processed in identical pipelines using edgeR v4.8 and limma v3.66. Lowly expressed genes were filtered with *filterByExpr*, libraries normalised by TMM, and voom precision-weighting was followed by *lmFit* with a means parameterisation (~0 + Group). Eight prespecified contrasts were tested via *makeContrasts* / *eBayes*: (i) Ctrl LPS response; (ii) basal GWI effect; (iii) GWI effect under LPS; (iv) GWI LPS response; (v) GWI × LPS interaction (Δ-LPS); (vi) basal CBD effect within GWI; (vii) CBD effect under LPS within GWI; (viii) CBD × LPS interaction within GWI. DEGs were called at Padj < 0.05 with $|\log_2 FC| > 0.5$; relaxed $P < 0.05$ thresholds were reported where indicated. Pathway analysis used clusterProfiler v4.18

(GO:BP, KEGG, MSigDB Hallmark via msigdbr v26.1, org.Mm.eg.db v3.22) in two modes: ORA on DEG sets and pre-ranked GSEA on signed $-\log_{10}$ p ranked lists. Pathway hits were declared consistent if they appeared in ≥ 2 of four DEG-threshold strata or in any single stratum plus the GSEA call for the same comparison and direction.

Cell-type module scores were computed on voom-normalised expression z-scored across samples; member-gene scores were averaged, modules with < 50% gene detection were flagged LOW_DETECTION, and contrast Δ values were tested with two-sample t-tests (**Supplementary Table S12**).

Acknowledgements

We thank Ga Hyun Kim for her help with mouse injections and animal care.

Funding

This study was supported by Congressionally Directed Medical Research Programs (CDMRP; the USA Department of the Army, Award No. GW210033/W81XWH-22-1-0172 [to K.-M.J.] and TX240175/ HT9425-25-1-0453 [to K.-M.J.].

Competing interest

All authors declare no competing interests.

Author information

Hye-Lim Lee and Heidi C. Avalos contributed equally.

Author contributions

KMJ conceived and designed the majority of the experiments, analyzed data, and wrote the manuscript. HLL and HCA designed, performed, and contributed to data analysis and manuscript preparation. JH and ES carried out the experiments and contributed to manuscript preparation. KMJ and DP supervised the overall study, obtained funding, oversaw data analysis and interpretation, and wrote the manuscript with input from all authors.

Figure Legends

Figure 1. Single-nucleus transcriptomic atlas of the aged GWI hippocampus.

(**a**) Schematic of the comparative transcriptome analysis between brain from control and GWI mice: hippocampus for snRNA-seq, whole-brain or FACS-purified microglia for bulk RNA-seq analyses. (**b**) UMAP of 37,745 high-quality nuclei, Harmony-integrated and colored by nine broad cell-type lineages. (**c**) UMAP split by condition: control (Ctrl) and GWI. (**d**) Dot plot of canonical lineage markers (*Slc17a7, Gad2, Mbp, Pdgfra, Aqp4, Cx3cr1, Cldn5, Pdgfrb*); dot size = fraction of nuclei expressing each marker, color = mean expression. (**e**) Stacked bar of broad-lineage composition per condition (n = 19,115 for Ctrl; and n = 18,630 for GWI). (**f**) Number of pathways with significant enrichment by GSEA, summarized by GO:BP, KEGG, and Hallmark categories on the broad cell-type clusters.

Figure 2. A multi-lineage primed-neuroimmune signature in the aged GWI hippocampus.

(**a, b**) Pre-ranked GSEA GO:BP results for microglial cluster from the broad lineage (**a**) and homeostatic microglia (Micro-Homeo) cluster from the fine cell type cluster (**b**), with leading-edge microglial genes shown in (**c**). (**d, e**) GSEA GO:BP results for oligodendrocyte progenitor cells (OPC) (**d**), and inhibitory neurons (Inh Neurons) (**e**). (**f**) Cell-type module score matrix showing pseudobulk z-score differences (GWI − Ctrl) for 39 functional modules (rows) across eight broad cell-type lineages (columns); modules with < 50% marker gene detection in a lineage are masked. Gray shading indicates modules that are not relevant to the corresponding cell type.

Figure 3. Whole-brain bulk RNA-seq reveals an amplified parenchymal response to systemic LPS in the aged GWI brain.

(**a, b**) PCA and volcano plots for the comparative analysis of GWI effects under (**a**) basal (PBS) and (**b**) immune-stimulated (LPS) conditions (n = 3-4 per group). (**c**) Basal GWI signature: pre-ranked GSEA-GO:BP results showing elevated cytoplasmic translation and reduced mRNA

processing. (**d**) Number of GO:BP terms significantly enriched in DEGs from over-representation analysis (ORA) comparing LPS- versus PBS-treated GWI and control mice across a range of statistical stringencies. (**e**) Immune-stimulated GWI signature: pre-ranked GSEA highlighting elevated leukocyte-mediated immunity and positive regulation of innate immune response. (**f**) Heatmap illustrating gene-level alterations in GWI versus control brains across basal and LPS-stimulated conditions; values indicate the $\log_2$[GWI/Ctrl] for each gene. (**g**) GSEA-GO:BP results for the formal ΔLPS interaction, resolving a GWI-amplified positive arm (leukocyte-mediated immunity and regulation of innate immune response) and a GWI-amplified negative arm (translation at synapse/presynapse/postsynapse and cytoplasmic translation). (**h**) Leading-edge gene panels for the formal ΔLPS interaction, showing the vascular/BBB/leukocyte-engagement arm (*Icam1, Pecam1, Itgb2*) and ribosomal-protein gene families with their $\log_2$[LPS/PBS] values.

Figure 4. GWI Microglia mount a blunted transcriptional response to systemic LPS — the microglial-exhaustion phenotype.

(**a, b**) PCA and volcano plots for the comparative analysis for GWI effects under (**a**) basal (PBS) and (**b**) immune-stimulated (LPS) conditions (n = 3-4 per group). (**c**) Basal GWI microglia signature: pre-ranked GSEA-GO:BP showing elevated translation at synapse, ribosome, and oxidative phosphorylation categories in GWI microglia at baseline. (**d**) Number of GO:BP terms significantly enriched in DEGs from over-representation analysis (ORA) comparing LPS- versus PBS-treated GWI and control mice across a range of statistical stringencies. (**e**) Microglial cell-type module score panel across the four experimental groups: in control mice, LPS drives the canonical decrease in Homeostatic and increases in Complement, Interferon_Antiviral, and Phagocytosis_Lysosome modules, whereas in GWI none of these reach significance and Antigen_Presentation and Lipid_DAM modules respond to LPS in the opposite direction. (**f, g**) Immune-stimulated GWI microglia signature: pre-ranked GSEA-GO:BP showing reduced proton motive force-driven ATP synthesis, mitochondrial translation, ATP biosynthetic process, and

oxidative phosphorylation (**f**), with leading-edge gene panels and corresponding $\log_2$[GWI/Ctrl] values in (**g**). (**h, i**) Pre-ranked GSEA summary of the formal GWI × LPS interaction (ΔLPS) within microglia, revealing reduced ribosome, oxidative phosphorylation, and translation at synapse pathways in GWI microglia (**h**) and leading-edge genes spanning ribosomal proteins, MHC molecules, and interferon-stimulated genes (**i**).

Figure 5. Chronic CBD partially rescues both arms of the GWI dual phenotype.

(**a**) Schematic of the CBD treatment paradigm: daily intraperitoneal CBD or vehicle for 28 days beginning 15 months after the GW chemicals exposure, followed by a single intraperitoneal LPS or PBS injection and tissue collection for bulk RNA-seq analysis of whole-brain and FACS-purified microglia. (**b**) Pre-ranked GSEA-GO:BP pathways down-regulated in whole brain by CBD, including translation at synapse and oxidative phosphorylation. (**c**) Top GSEA-GO:BP categories down-regulated in whole brain by CBD under LPS, led by antigen processing and presentation, leukocyte-mediated immunity, and lymphocyte/adaptive immunity. (**d**) GSEA-GO:BP results in LPS-stimulated microglia showing CBD-induced elevation of meiotic cell cycle program and reduction of ribosome biogenesis genes. (**e**) Functional module analysis indicating CBD-provided rescue of Antigen_Presentation and Interferon_Antiviral signatures in LPS-stimulated GWI microglia. (**f**) Formal CBD × LPS interaction in microglia revealing increased ATP synthesis, oxidative phosphorylation, and ribosome pathways driven by *Rpl/Rps/Mrpl/Mrps* gene families (**g**), alongside concurrent down-regulation of GO:BP ribosome biogenesis terms (**f**) driven by upstream regulators (**g**).

Supplementary information

The following items will be provided as Supplementary information files.

Supplementary Figures S1-S12

Supplementary Figure S1. Fine cell-type annotation of the hippocampal snRNA-seq atlas.

Supplementary Figure S2. Expression of canonical lineage markers.

Supplementary Figure S3. Hallmark pathway enrichment in broad cell-type clusters.

Supplementary Figure S4. Hallmark pathway enrichment in selected fine cell-type clusters.

Supplementary Figure S5. Glycolytic gene expression across microglia clusters.

Supplementary Figure S6. Whole-brain bulk RNA-seq GSEA-KEGG enrichment for GWI.

Supplementary Figure S7. Brain-wide response to LPS stimulation in aged control and GWI mice.

Supplementary Figure S8. Microglia bulk RNA-seq GSEA-KEGG and GSEA-GO:BP enrichment for GWI.

Supplementary Figure S9. Microglial response to LPS stimulation in aged control and GWI mice.

Supplementary Figure S10. Brain-wide response to CBD treatment in aged GWI mice.

Supplementary Figure S11. Microglial response to CBD treatment in aged GWI mice.

Supplementary Figure S12. Effects of CBD treatment on endocannabinoid (ECB)-related genes in GWI mice.

Supplementary Tables S1-S12

Supplementary Table S1. Counts for the broad and fine cell-type clusters and associated markers

(Excel file: Table_S1_Summary_snRNAseq_cell_annotation.xlsx)

Supplementary Table S2. Counts for GSEA results in broad and fine cell-type clusters

(Excel file: Table_S2_Summary_GSEA_snRNAseq_CellType.xlsx)

Supplementary Table S3. Functional module analysis for broad cell-type clusters

(Excel file: Table_S3_Global_module_analysis.xlsx)

Supplementary Table S4. DEG analysis summary for the brain-wide bulk RNA-seq dataset

(Excel file: Table_S4_Brainwide_DEG_GO_KEGG_summary_counts.xlsx)

Supplementary Table S5. Significant GO:BP terms for LPS-upregulated DEGs from brain-wide bulk RNA-seq

(Excel file: Table_S5_Brainwide_LPS_Effects_UpDEG_GO_BP)

Supplementary Table S6. Brainwide GSEA-GO:BP and GSEA-KEGG analyses for the ΔLPS interaction

(Excel file: Table_S6_Brainwide_delta_LPS_GSEA_GO_BP_KEGG.xlsx)

Supplementary Table S7. DEG analysis summary for the microglia bulk RNA-seq dataset

(Excel file: Table_S7_Microglia_DEG_GO_KEGG_summary_counts.xlsx)

Supplementary Table S8. Significant GO:BP terms for LPS-upregulated DEGs from microglia bulk RNA-seq

(Excel file: Table_S8_Microglia_LPS_Effects_UpDEG_GO_BP.xlsx)

Supplementary Table S9. Significant GO:BP terms for CBD-downregulated DEGs from brain-wide bulk RNA-seq in GWI-LPS mice

(Excel file: Table_S9_Brainwide_CBD_Effects_DownDEG_GWI_LPS_GO_BP.xlsx)

Supplementary Table S10. Significant GO:BP terms for CBD-upregulated and CBD-downregulated DEGs from microglia bulk RNA-seq in GWI-LPS mice

(Excel file: Table_S10_Microglia_CBD_Effects_Down_Up_DEG_GWI_LPS_GO_BP.xlsx)

Supplementary Table S11. GSEA-GO:BP and GSEA-KEGG analyses for the effects of CBD on microglia for the ΔLPS interaction in GWI mice

(Excel file: Table_S11_Microglia_CBD_Effects_GWI_LPS_GSEA_GOBP_KEGG.xlsx)

Supplementary Table S12. List of marker genes for the cell-type selective functional module analysis

(Excel file: Table_S12_List_Celltype_Module_Genes.xlsx)

Source data

A Source Data file containing the underlying values for every panel of Figures 1–5 will be provided.

Data availability

Raw sequencing reads and processed count/expression matrices from snRNA-seq, whole-brain bulk RNA-seq, and FACS-purified microglia bulk RNA-seq generated in this study will be deposited to an online depository before the publication.

Code availability

The complete analysis pipeline (R scripts for snRNA-seq processing, bulk RNA-seq differential expression, pathway enrichment, and cell-type module scoring) will be deposited to an online depository before the publication.

References

1 Programs, C. D. M. R. *Gulf War Illness Research Program*, <https://cdmrp.health.mil/gwirp/> (

2 Fukuda, K. Chronic multisymptom illness affecting Air Force veterans of the Gulf War. *JAMA* **280**, 981-988 (1998).

3 Binns, J. H. *Gulf War Illness and the Health of Gulf War Veterans*. (Research Advisory Committee on Gulf War Veterans' Illnesses, 2008).

4 Steele, L. Prevalence and patterns of Gulf War illness in Kansas veterans: association of symptoms with characteristics of person, place, and time of military service. *Am J Epidemiol* **152**, 992-1002 (2000). https://doi.org/10.1093/aje/152.10.992

5 White, R. F. *et al.* Recent research on Gulf War illness and other health problems in veterans of the 1991 Gulf War: Effects of toxicant exposures during deployment. *Cortex* **74**, 449-475 (2016). https://doi.org/10.1016/j.cortex.2015.08.022

6 Illnesses, R. A. C. o. G. W. V. Gulf War Illness and the Health of Gulf War Veterans: Scientific Findings and Recommendations. (Washington, D.C., 2008).

7 Attaluri, S. Brain-specific increase in leukotriene signaling accompanies chronic neuroinflammation and cognitive impairment in a model of Gulf War Illness. *Frontiers in Immunology* **13**, 853000 (2022).

8 Zakirova, Z. A chronic longitudinal characterization of neurobehavioral and neuropathological cognitive impairment in a mouse model of Gulf War agent exposure. *Frontiers in Integrative Neuroscience* **9**, 71 (2016).

9 Dickey, B., Madhu, L. N. & Shetty, A. K. Gulf War Illness: Mechanisms Underlying Brain Dysfunction and Promising Therapeutic Strategies. *Pharmacol Ther* **220**, 107716 (2021). https://doi.org/10.1016/j.pharmthera.2020.107716

10 Johnson, G. J., Leis, L. A., Slater, B. C. & Bach, R. R. Elevated platelet count, C-reactive protein and thromboxane analog-induced platelet aggregation in patients with Gulf War veterans' illnesses: evidence of a chronic inflammatory state? *Blood Coagul Fibrinolysis* **24**, 736-741 (2013). https://doi.org/10.1097/MBC.0b013e328362627f

11 Khaiboullina, S. F. *et al.* Cytokine expression provides clues to the pathophysiology of Gulf War illness and myalgic encephalomyelitis. *Cytokine* **72**, 1-8 (2015). https://doi.org/10.1016/j.cyto.2014.11.019

12 Janulewicz, P. A. *et al.* The Gut-Microbiome in Gulf War Veterans: A Preliminary Report. *Int J Environ Res Public Health* **16** (2019). https://doi.org/10.3390/ijerph16193751

13 Parkitny, L., Middleton, S., Baker, K. & Younger, J. Evidence for abnormal cytokine expression in Gulf War Illness: A preliminary analysis of daily immune monitoring data. *BMC Immunol* **16**, 57 (2015). https://doi.org/10.1186/s12865-015-0122-z

14 Alshelh, Z. In-vivo imaging of neuroinflammation in veterans with Gulf War illness. *Brain, Behavior, and Immunity* **87**, 498-507 (2020).

15 Madhu, L. N. Neuroinflammation in Gulf War Illness is linked with HMGB1 and complement activation. *Brain, Behavior, and Immunity* **81**, 430-443 (2019).

16 Keating, D. Circulating HMGB1 is elevated in veterans with Gulf War Illness and triggers the persistent pro-inflammatory microglia phenotype. *Brain, Behavior, and Immunity* **96**, 10-22 (2021).

17 Chao, L. L. The Prevalence of Mild Cognitive Impairment in a Convenience Sample of 202 Gulf War Veterans. *Int J Environ Res Public Health* **17** (2020). https://doi.org/10.3390/ijerph17197158

18 Chao, L. L. The prevalence of mild cognitive impairment in Gulf War veterans: a follow-up study. *Frontiers in Neuroscience* **17**, 1301066 (2023).

19 Carpenter, J. M., Hughes, S. N. & Filipov, N. M. Longitudinal evaluation of structural brain alterations in two established mouse models of Gulf War Illness. *Front Neurosci* **18**, 1465701 (2024). https://doi.org/10.3389/fnins.2024.1465701
20 Terry, A. V., Jr. *et al.* Acute exposure to diisopropylfluorophosphate in mice results in persistent cognitive deficits and alterations in senescence markers in the brain. *Front Neurosci* **18**, 1498350 (2024). https://doi.org/10.3389/fnins.2024.1498350
21 Tsai, Y. H. *et al.* Acute intoxication with diisopropylfluorophosphate promotes cellular senescence in the adult male rat brain. *Front Toxicol* **6**, 1360359 (2024). https://doi.org/10.3389/ftox.2024.1360359
22 Frank, M. G. Microglia priming with aging and stress. *Neuropsychopharmacology* **42**, 318-333 (2017).
23 Perry, V. H. & Holmes, C. Microglial priming in neurodegenerative disease. *Nat Rev Neurol* **10**, 217-224 (2014). https://doi.org/10.1038/nrneurol.2014.38
24 Squire, E. *et al.* Targeting dysfunctional endocannabinoid signaling in a mouse model of Gulf War illness. *Neuropharmacology* **261**, 110142 (2024). https://doi.org/10.1016/j.neuropharm.2024.110142
25 Millet, A., Ledo, J. H. & Tavazoie, S. F. An exhausted-like microglial population accumulates in aged and APOE4 genotype Alzheimer's brains. *Immunity* **57**, 153-170 e156 (2024). https://doi.org/10.1016/j.immuni.2023.12.001
26 Leweke, F. M. *et al.* Cannabidiol enhances anandamide signaling and alleviates psychotic symptoms of schizophrenia. *Transl Psychiatry* **2**, e94 (2012). https://doi.org/10.1038/tp.2012.15
27 Dos-Santos-Pereira, M., Guimaraes, F. S., Del-Bel, E., Raisman-Vozari, R. & Michel, P. P. Cannabidiol prevents LPS-induced microglial inflammation by inhibiting ROS/NF-kappaB-dependent signaling and glucose consumption. *Glia* **68**, 561-573 (2020). https://doi.org/10.1002/glia.23738
28 Kodali, M. *et al.* FDA-approved cannabidiol [Epidiolex((R))] alleviates Gulf War Illness-linked cognitive and mood dysfunction, hyperalgesia, neuroinflammatory signaling, and declined neurogenesis. *Mil Med Res* **11**, 61 (2024). https://doi.org/10.1186/s40779-024-00563-2
29 Baik, S. H. *et al.* A Breakdown in Metabolic Reprogramming Causes Microglia Dysfunction in Alzheimer's Disease. *Cell Metab* **30**, 493-507 e496 (2019). https://doi.org/10.1016/j.cmet.2019.06.005
30 Sabogal-Guaqueta, A. M. *et al.* Species-specific metabolic reprogramming in human and mouse microglia during inflammatory pathway induction. *Nat Commun* **14**, 6454 (2023). https://doi.org/10.1038/s41467-023-42096-7
31 Patani, R., Hardingham, G. E. & Liddelow, S. A. Functional roles of reactive astrocytes in neuroinflammation and neurodegeneration. *Nat Rev Neurol* **19**, 395-409 (2023). https://doi.org/10.1038/s41582-023-00822-1
32 Yuan, B. *et al.* Neutrophils-astrocyte interactions in central nervous system inflammation. *Cell Death Dis* **16**, 643 (2025). https://doi.org/10.1038/s41419-025-07945-x
33 Zenaro, E. *et al.* Neutrophils promote Alzheimer's disease-like pathology and cognitive decline via LFA-1 integrin. *Nat Med* **21**, 880-886 (2015). https://doi.org/10.1038/nm.3913
34 Parihar, V. K., Hattiangady, B., Shuai, B. & Shetty, A. K. Mood and memory deficits in a model of Gulf War illness are linked with reduced neurogenesis, partial neuron loss, and mild inflammation in the hippocampus. *Neuropsychopharmacology* **38**, 2348-2362 (2013). https://doi.org/10.1038/npp.2013.158
35 Kodali, M. *et al.* Curcumin treatment leads to better cognitive and mood function in a model of Gulf War Illness with enhanced neurogenesis, and alleviation of inflammation and mitochondrial dysfunction in the hippocampus. *Brain Behav Immun* **69**, 499-514 (2018). https://doi.org/10.1016/j.bbi.2018.01.009

36 Wendeln, A. C. *et al.* Innate immune memory in the brain shapes neurological disease hallmarks. *Nature* **556**, 332-338 (2018). https://doi.org/10.1038/s41586-018-0023-4
37 Pluvinage, J. V. *et al.* CD22 blockade restores homeostatic microglial phagocytosis in ageing brains. *Nature* **568**, 187-192 (2019). https://doi.org/10.1038/s41586-019-1088-4
38 Hammond, T. R. *et al.* Single-Cell RNA Sequencing of Microglia throughout the Mouse Lifespan and in the Injured Brain Reveals Complex Cell-State Changes. *Immunity* **50**, 253-271 e256 (2019). https://doi.org/10.1016/j.immuni.2018.11.004
39 Streit, W. J. Dystrophic (senescent) rather than activated microglial cells are associated with tau pathology and likely precede neurodegeneration in Alzheimer's disease. *Acta Neuropathologica* **118**, 475-485 (2009).
40 Graeber, M. B. & Streit, W. J. Microglia: biology and pathology. *Acta Neuropathol* **119**, 89-105 (2010). https://doi.org/10.1007/s00401-009-0622-0
41 Keren-Shaul, H. *et al.* A Unique Microglia Type Associated with Restricting Development of Alzheimer's Disease. *Cell* **169**, 1276-1290 e1217 (2017). https://doi.org/10.1016/j.cell.2017.05.018
42 Sala Frigerio, C. *et al.* The Major Risk Factors for Alzheimer's Disease: Age, Sex, and Genes Modulate the Microglia Response to Abeta Plaques. *Cell Rep* **27**, 1293-1306 e1296 (2019). https://doi.org/10.1016/j.celrep.2019.03.099
43 Olah, M. *et al.* Single cell RNA sequencing of human microglia uncovers a subset associated with Alzheimer's disease. *Nat Commun* **11**, 6129 (2020). https://doi.org/10.1038/s41467-020-19737-2
44 Fernandez-Castaneda, A. *et al.* Mild respiratory COVID can cause multi-lineage neural cell and myelin dysregulation. *Cell* **185**, 2452-2468 e2416 (2022). https://doi.org/10.1016/j.cell.2022.06.008
45 Zhang, T. *et al.* Brain-wide alterations revealed by spatial transcriptomics and proteomics in COVID-19 infection. *Nat Aging* **4**, 1598-1618 (2024). https://doi.org/10.1038/s43587-024-00730-z
46 Van Hove, H. *et al.* A single-cell atlas of mouse brain macrophages reveals unique transcriptional identities shaped by ontogeny and tissue environment. *Nat Neurosci* **22**, 1021-1035 (2019). https://doi.org/10.1038/s41593-019-0393-4
47 Mrdjen, D. *et al.* High-Dimensional Single-Cell Mapping of Central Nervous System Immune Cells Reveals Distinct Myeloid Subsets in Health, Aging, and Disease. *Immunity* **48**, 380-395 e386 (2018). https://doi.org/10.1016/j.immuni.2018.01.011
48 Lee, H. L. *et al.* Frequent Low-Dose Delta(9)-Tetrahydrocannabinol in Adolescence Disrupts Microglia Homeostasis and Disables Responses to Microbial Infection and Social Stress in Young Adulthood. *Biol Psychiatry* **92**, 845-860 (2022). https://doi.org/10.1016/j.biopsych.2022.04.017

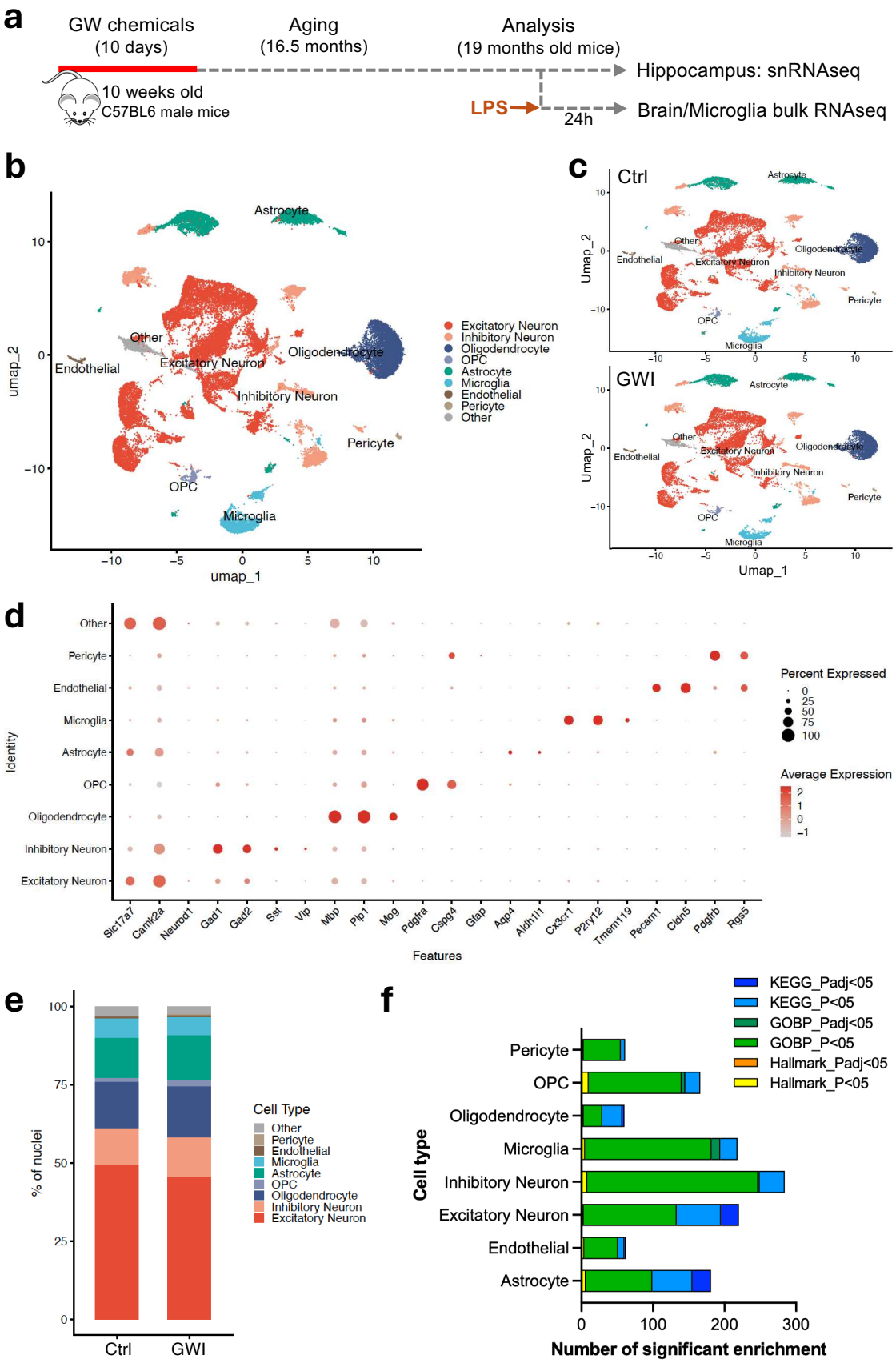
a
GW chemicals
(10 days)
Aging
(16.5 months)
Analysis
(19 months old mice)
10 weeks old
C57BL6 male mice
Hippocampus: snRNAseq
LPS
24h
Brain/Microglia bulk RNAseq
b
Astrocyte
Other
Excitatory Neuron
Oligodendrocyte
Endothelial
Inhibitory Neuron
Pericyte
OPC
Microglia
umap_1
umap_2
Excitatory Neuron
Inhibitory Neuron
Oligodendrocyte
OPC
Astrocyte
Microglia
Endothelial
Pericyte
Other
c
Ctrl
GWI
Umap_1
Umap_2
d
Identity
Features
Percent Expressed
Average Expression
Slc17a7
Camk2a
Neurod1
Gad1
Gad2
Sst
Vip
Mbp
Plp1
Mog
Pdgfra
Cspg4
Gfap
Aqp4
Aldh1l1
Cx3cr1
P2ry12
Tmem119
Pecam1
Cldn5
Pdgfrb
Rgs5
e
% of nuclei
Ctrl
GWI
Cell Type
f
KEGG_Padj<05
KEGG_P<05
GOBP_Padj<05
GOBP_P<05
Hallmark_Padj<05
Hallmark_P<05
Cell type
Number of significant enrichment

Figure 1

Figure 1. Single-nucleus transcriptomic atlas of the aged GWI hippocampus.

(**a**) Schematic of the comparative transcriptome analysis between brain from control and GWI mice: hippocampus for snRNA-seq, whole-brain or FACS-purified microglia for bulk RNA-seq analyses. (**b**) UMAP of 37,745 high-quality nuclei, Harmony-integrated and colored by nine broad cell-type lineages. (**c**) UMAP split by condition: control (Ctrl) and GWI. (**d**) Dot plot of canonical lineage markers (*Slc17a7, Gad2, Mbp, Pdgfra, Aqp4, Cx3cr1, Cldn5, Pdgfrb*); dot size = fraction of nuclei expressing each marker, color = mean expression. (**e**) Stacked bar of broad-lineage composition per condition (n = 19,115 for Ctrl; and n = 18,630 for GWI). (**f**) Number of pathways with significant enrichment by GSEA, summarized by GO:BP, KEGG, and Hallmark categories on the broad cell-type clusters.

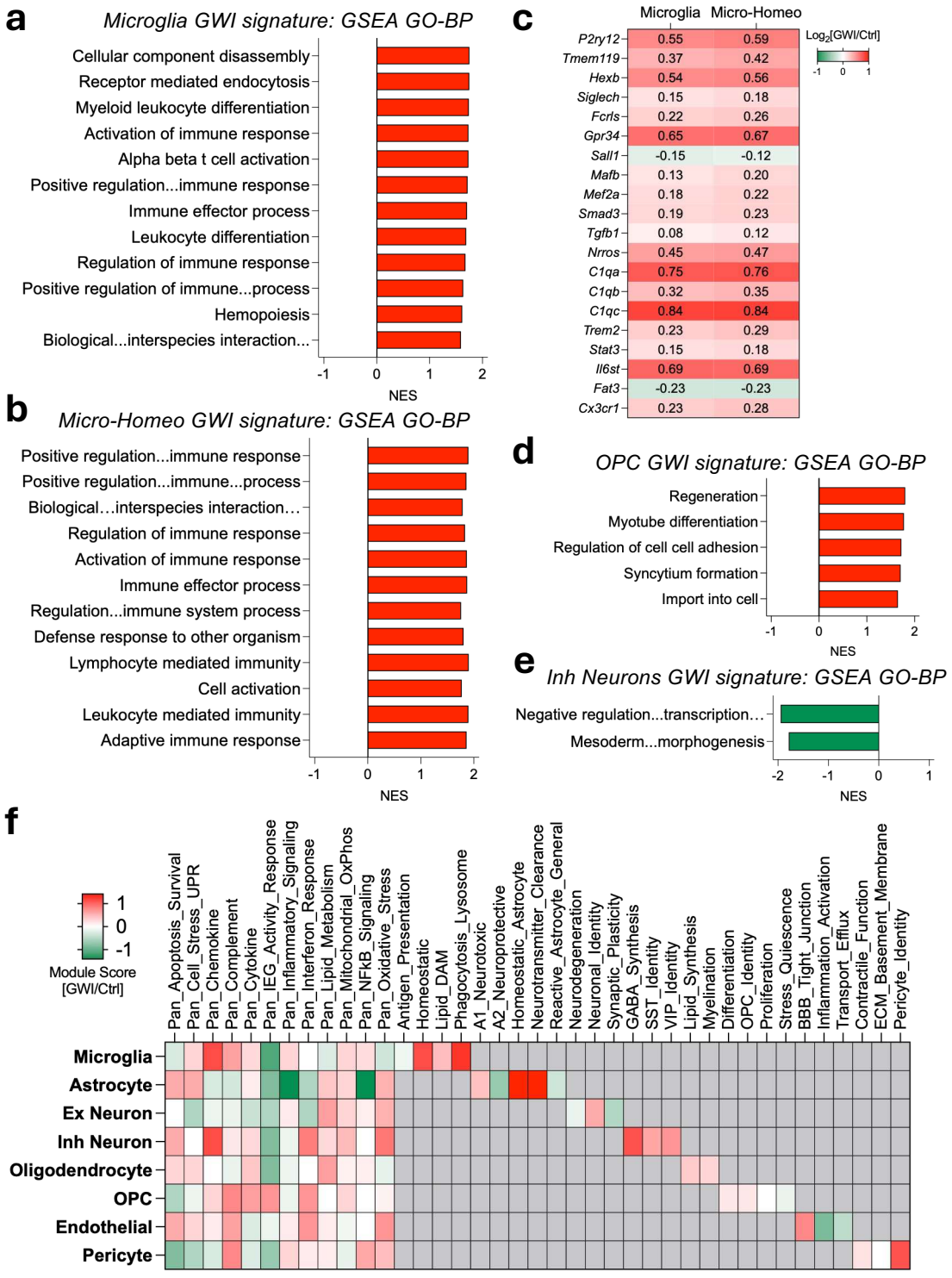
a
Microglia GWI signature: GSEA GO-BP
Cellular component disassembly
Receptor mediated endocytosis
Myeloid leukocyte differentiation
Activation of immune response
Alpha beta t cell activation
Positive regulation...immune response
Immune effector process
Leukocyte differentiation
Regulation of immune response
Positive regulation of immune...process
Hemopoiesis
Biological...interspecies interaction...
-1 0 1 2
NES
b
Micro-Homeo GWI signature: GSEA GO-BP
Positive regulation...immune response
Positive regulation...immune...process
Biological…interspecies interaction…
Regulation of immune response
Activation of immune response
Immune effector process
Regulation...immune system process
Defense response to other organism
Lymphocyte mediated immunity
Cell activation
Leukocyte mediated immunity
Adaptive immune response
-1 0 1 2
NES
c
Microglia Micro-Homeo
Log2[GWI/Ctrl]
-1 0 1
P2ry12 0.55 0.59
Tmem119 0.37 0.42
Hexb 0.54 0.56
Siglech 0.15 0.18
Fcrls 0.22 0.26
Gpr34 0.65 0.67
Sall1 -0.15 -0.12
Mafb 0.13 0.20
Mef2a 0.18 0.22
Smad3 0.19 0.23
Tgfb1 0.08 0.12
Nrros 0.45 0.47
C1qa 0.75 0.76
C1qb 0.32 0.35
C1qc 0.84 0.84
Trem2 0.23 0.29
Stat3 0.15 0.18
Il6st 0.69 0.69
Fat3 -0.23 -0.23
Cx3cr1 0.23 0.28
d
OPC GWI signature: GSEA GO-BP
Regeneration
Myotube differentiation
Regulation of cell cell adhesion
Syncytium formation
Import into cell
-1 0 1 2
NES
e
Inh Neurons GWI signature: GSEA GO-BP
Negative regulation...transcription…
Mesoderm...morphogenesis
-2 -1 0 1
NES
f
1
0
-1
Module Score [GWI/Ctrl]
Pan_Apoptosis_Survival
Pan_Cell_Stress_UPR
Pan_Chemokine
Pan_Complement
Pan_Cytokine
Pan_IEG_Activity_Response
Pan_Inflammatory_Signaling
Pan_Interferon_Response
Pan_Lipid_Metabolism
Pan_Mitochondrial_OxPhos
Pan_NFkB_Signaling
Pan_Oxidative_Stress
Antigen_Presentation
Homeostatic
Lipid_DAM
Phagocytosis_Lysosome
A1_Neurotoxic
A2_Neuroprotective
Homeostatic_Astrocyte
Neurotransmitter_Clearance
Reactive_Astrocyte_General
Neurodegeneration
Neuronal_Identity
Synaptic_Plasticity
GABA_Synthesis
SST_Identity
VIP_Identity
Lipid_Synthesis
Myelination
Differentiation
OPC_Identity
Proliferation
Stress_Quiescence
BBB_Tight_Junction
Inflammation_Activation
Transport_Efflux
Contractile_Function
ECM_Basement_Membrane
Pericyte_Identity
Microglia
Astrocyte
Ex Neuron
Inh Neuron
Oligodendrocyte
OPC
Endothelial
Pericyte

Figure 2

Figure 2. A multi-lineage primed-neuroimmune signature in the aged GWI hippocampus.
(**a, b**) Pre-ranked GSEA GO:BP results for microglial cluster from the broad lineage (**a**) and homeostatic microglia (Micro-Homeo) cluster from the fine cell type cluster (**b**), with leading-edge microglial genes shown in (**c**). (**d, e**) GSEA GO:BP results for oligodendrocyte progenitor cells (OPC) (**d**), and inhibitory neurons (Inh Neurons) (**e**). (**f**) Cell-type module score matrix showing pseudobulk z-score differences (GWI − Ctrl) for 39 functional modules (rows) across eight broad cell-type lineages (columns); modules with < 50% marker gene detection in a lineage are masked. Gray shading indicates modules that are not relevant to the corresponding cell type.

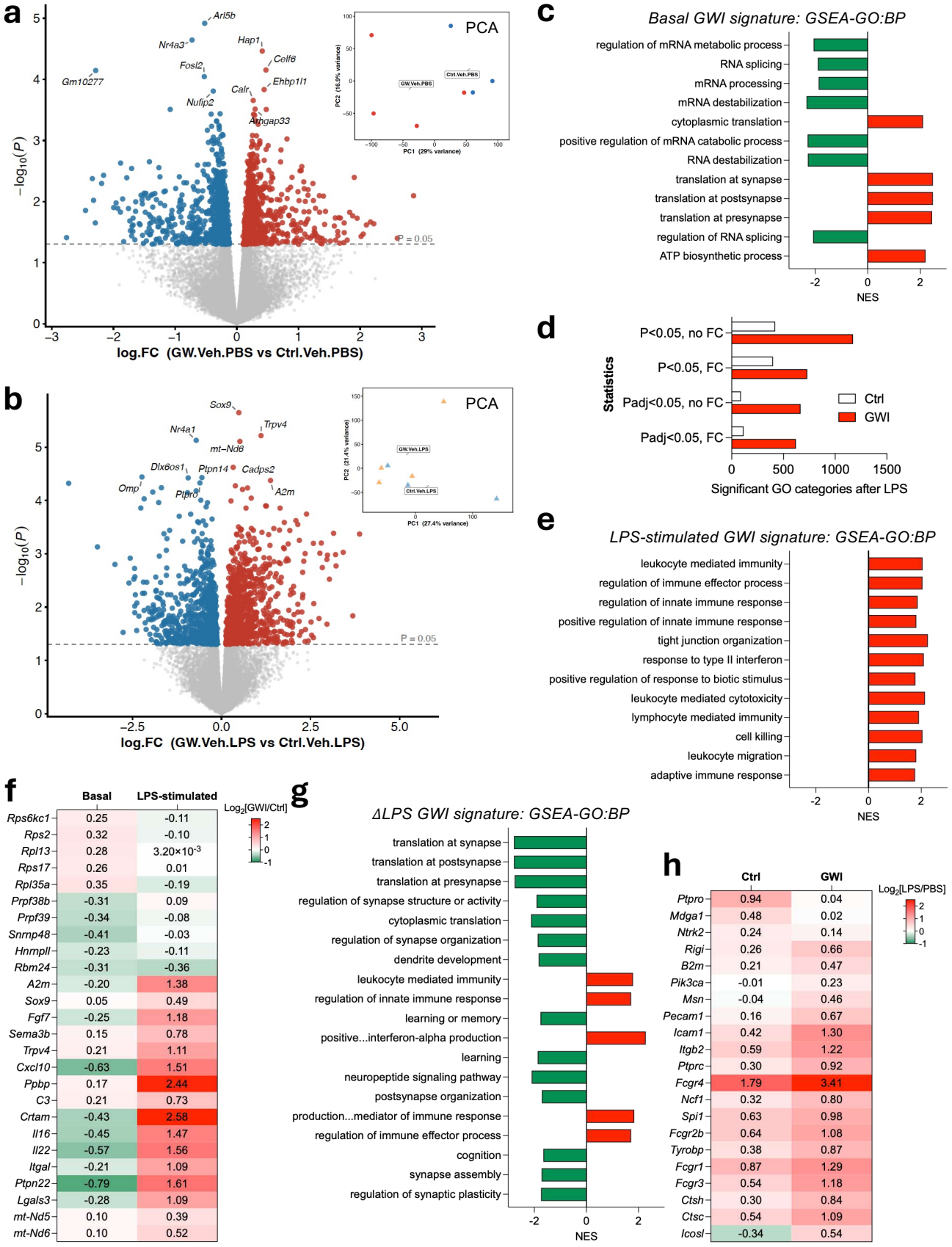
a
PCA
Arl5b
Nr4a3
Hap1
Celf6
Fosl2
Gm10277
Ehbp1l1
Calr
Nufip2
Arhgap33
P = 0.05
log.FC (GW.Veh.PBS vs Ctrl.Veh.PBS)
b
PCA
Sox9
Nr4a1
Trpv4
mt-Nd6
Dlx6os1
Ptpn14
Cadps2
Omp
Ptprd
A2m
P = 0.05
log.FC (GW.Veh.LPS vs Ctrl.Veh.LPS)
c
Basal GWI signature: GSEA-GO:BP
regulation of mRNA metabolic process
RNA splicing
mRNA processing
mRNA destabilization
cytoplasmic translation
positive regulation of mRNA catabolic process
RNA destabilization
translation at synapse
translation at postsynapse
translation at presynapse
regulation of RNA splicing
ATP biosynthetic process
NES
d
Statistics
P<0.05, no FC
P<0.05, FC
Padj<0.05, no FC
Padj<0.05, FC
Ctrl
GWI
Significant GO categories after LPS
e
LPS-stimulated GWI signature: GSEA-GO:BP
leukocyte mediated immunity
regulation of immune effector process
regulation of innate immune response
positive regulation of innate immune response
tight junction organization
response to type II interferon
positive regulation of response to biotic stimulus
leukocyte mediated cytotoxicity
lymphocyte mediated immunity
cell killing
leukocyte migration
adaptive immune response
NES
f
Basal
LPS-stimulated
Log2[GWI/Ctrl]
Rps6kc1 0.25 -0.11
Rps2 0.32 -0.10
Rpl13 0.28 3.20×10-3
Rps17 0.26 0.01
Rpl35a 0.35 -0.19
Prpf38b -0.31 0.09
Prpf39 -0.34 -0.08
Snrnp48 -0.41 -0.03
Hnrnpll -0.23 -0.11
Rbm24 -0.31 -0.36
A2m -0.20 1.38
Sox9 0.05 0.49
Fgf7 -0.25 1.18
Sema3b 0.15 0.78
Trpv4 0.21 1.11
Cxcl10 -0.63 1.51
Ppbp 0.17 2.44
C3 0.21 0.73
Crtam -0.43 2.58
Il16 -0.45 1.47
Il22 -0.57 1.56
Itgal -0.21 1.09
Ptpn22 -0.79 1.61
Lgals3 -0.28 1.09
mt-Nd5 0.10 0.39
mt-Nd6 0.10 0.52
g
ΔLPS GWI signature: GSEA-GO:BP
translation at synapse
translation at postsynapse
translation at presynapse
regulation of synapse structure or activity
cytoplasmic translation
regulation of synapse organization
dendrite development
leukocyte mediated immunity
regulation of innate immune response
learning or memory
positive...interferon-alpha production
learning
neuropeptide signaling pathway
postsynapse organization
production...mediator of immune response
regulation of immune effector process
cognition
synapse assembly
regulation of synaptic plasticity
NES
h
Ctrl
GWI
Log2[LPS/PBS]
Ptpro 0.94 0.04
Mdga1 0.48 0.02
Ntrk2 0.24 0.14
Rigi 0.26 0.66
B2m 0.21 0.47
Pik3ca -0.01 0.23
Msn -0.04 0.46
Pecam1 0.16 0.67
Icam1 0.42 1.30
Itgb2 0.59 1.22
Ptprc 0.30 0.92
Fcgr4 1.79 3.41
Ncf1 0.32 0.80
Spi1 0.63 0.98
Fcgr2b 0.64 1.08
Tyrobp 0.38 0.87
Fcgr1 0.87 1.29
Fcgr3 0.54 1.18
Ctsh 0.30 0.84
Ctsc 0.54 1.09
Icosl -0.34 0.54

Figure 3

Figure 3. Whole-brain bulk RNA-seq reveals an amplified parenchymal response to systemic LPS in the aged GWI brain.

(**a, b**) PCA and volcano plots for the comparative analysis of GWI effects under (**a**) basal (PBS) and (**b**) immune-stimulated (LPS) conditions (n = 3-4 per group). (**c**) Basal GWI signature: pre-ranked GSEA-GO:BP results showing elevated cytoplasmic translation and reduced mRNA processing. (**d**) Number of GO:BP terms significantly enriched in DEGs from over-representation analysis (ORA) comparing LPS- versus PBS-treated GWI and control mice across a range of statistical stringencies. (**e**) Immune-stimulated GWI signature: pre-ranked GSEA highlighting elevated leukocyte-mediated immunity and positive regulation of innate immune response. (**f**) Heatmap illustrating gene-level alterations in GWI versus control brains across basal and LPS-stimulated conditions; values indicate the $\log_2$[GWI/Ctrl] for each gene. (**g**) GSEA-GO:BP results for the formal ΔLPS interaction, resolving a GWI-amplified positive arm (leukocyte-mediated immunity and regulation of innate immune response) and a GWI-amplified negative arm (translation at synapse/presynapse/postsynapse and cytoplasmic translation). (**h**) Leading-edge gene panels for the formal ΔLPS interaction, showing the vascular/BBB/leukocyte-engagement arm (*Icam1, Pecam1, Itgb2*) and ribosomal-protein gene families with their $\log_2$[LPS/PBS] values.

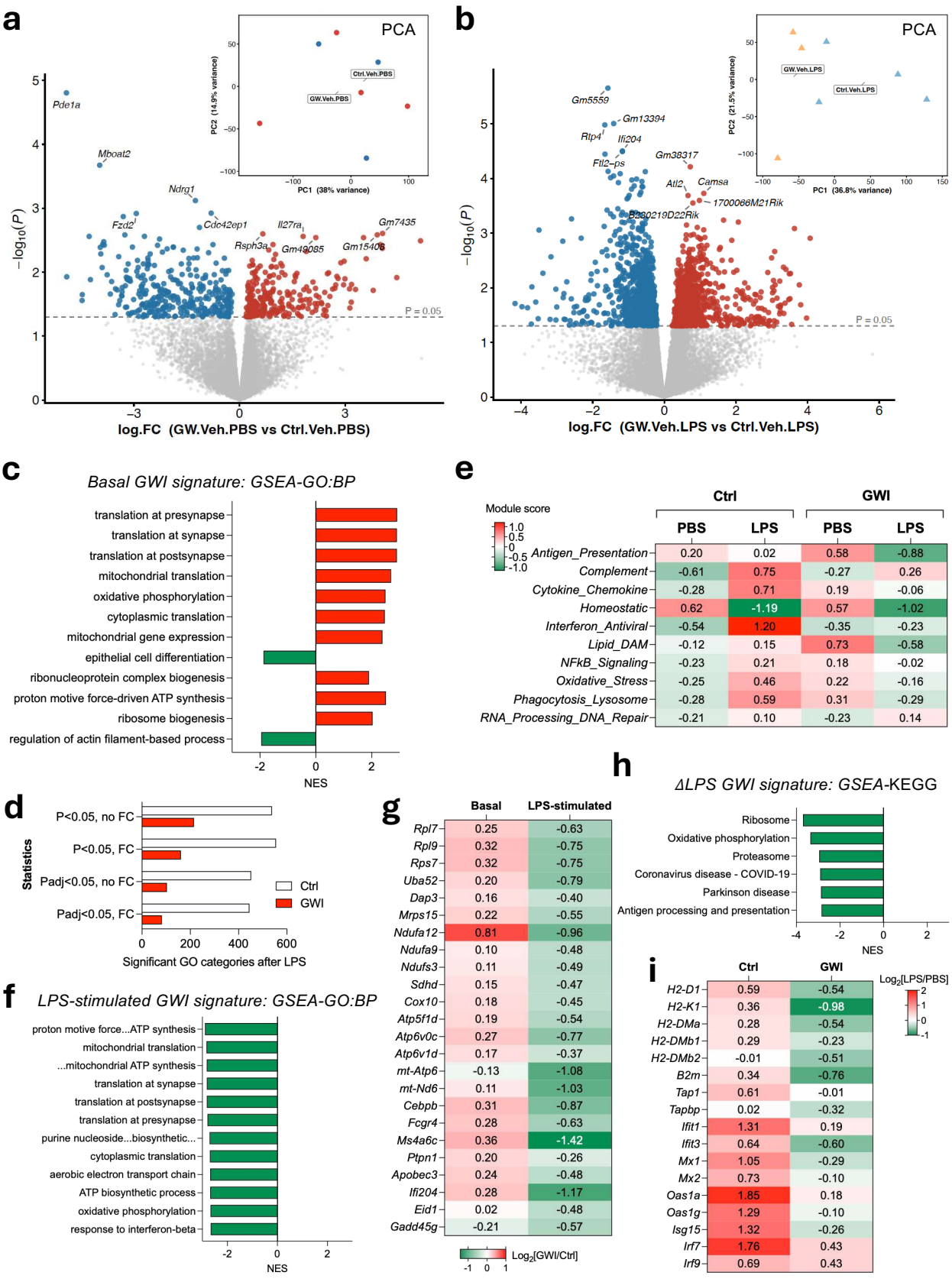
a
PCA
Ctrl.Veh.PBS
GW.Veh.PBS
PC1 (38% variance)
PC2 (14.9% variance)
Pde1a
Mboat2
Ndrg1
Fzd2
Cdc42ep1
Il27ra
Rsph3a
Gm49085
Gm15406
Gm7435
P = 0.05
−log10(P)
log.FC (GW.Veh.PBS vs Ctrl.Veh.PBS)
b
PCA
GW.Veh.LPS
Ctrl.Veh.LPS
PC1 (36.8% variance)
PC2 (21.5% variance)
Gm5559
Gm13394
Rtp4
Ifi204
Ftl2−ps
Gm38317
Atl2
Camsa
1700086M21Rik
B230219D22Rik
P = 0.05
−log10(P)
log.FC (GW.Veh.LPS vs Ctrl.Veh.LPS)
c
Basal GWI signature: GSEA-GO:BP
translation at presynapse
translation at synapse
translation at postsynapse
mitochondrial translation
oxidative phosphorylation
cytoplasmic translation
mitochondrial gene expression
epithelial cell differentiation
ribonucleoprotein complex biogenesis
proton motive force-driven ATP synthesis
ribosome biogenesis
regulation of actin filament-based process
NES
d
P<0.05, no FC
P<0.05, FC
Padj<0.05, no FC
Padj<0.05, FC
Ctrl
GWI
Statistics
Significant GO categories after LPS
e
Module score
Ctrl
GWI
PBS
LPS
PBS
LPS
Antigen_Presentation 0.20 0.02 0.58 -0.88
Complement -0.61 0.75 -0.27 0.26
Cytokine_Chemokine -0.28 0.71 0.19 -0.06
Homeostatic 0.62 -1.19 0.57 -1.02
Interferon_Antiviral -0.54 1.20 -0.35 -0.23
Lipid_DAM -0.12 0.15 0.73 -0.58
NFkB_Signaling -0.23 0.21 0.18 -0.02
Oxidative_Stress -0.25 0.46 0.22 -0.16
Phagocytosis_Lysosome -0.28 0.59 0.31 -0.29
RNA_Processing_DNA_Repair -0.21 0.10 -0.23 0.14
f
LPS-stimulated GWI signature: GSEA-GO:BP
proton motive force...ATP synthesis
mitochondrial translation
...mitochondrial ATP synthesis
translation at synapse
translation at postsynapse
translation at presynapse
purine nucleoside...biosynthetic...
cytoplasmic translation
aerobic electron transport chain
ATP biosynthetic process
oxidative phosphorylation
response to interferon-beta
NES
g
Basal
LPS-stimulated
Rpl7 0.25 -0.63
Rpl9 0.32 -0.75
Rps7 0.32 -0.75
Uba52 0.20 -0.79
Dap3 0.16 -0.40
Mrps15 0.22 -0.55
Ndufa12 0.81 -0.96
Ndufa9 0.10 -0.48
Ndufs3 0.11 -0.49
Sdhd 0.15 -0.47
Cox10 0.18 -0.45
Atp5f1d 0.19 -0.54
Atp6v0c 0.27 -0.77
Atp6v1d 0.17 -0.37
mt-Atp6 -0.13 -1.08
mt-Nd6 0.11 -1.03
Cebpb 0.31 -0.87
Fcgr4 0.28 -0.63
Ms4a6c 0.36 -1.42
Ptpn1 0.20 -0.26
Apobec3 0.24 -0.48
Ifi204 0.28 -1.17
Eid1 0.02 -0.48
Gadd45g -0.21 -0.57
Log2[GWI/Ctrl]
h
ΔLPS GWI signature: GSEA-KEGG
Ribosome
Oxidative phosphorylation
Proteasome
Coronavirus disease - COVID-19
Parkinson disease
Antigen processing and presentation
NES
i
Ctrl
GWI
Log2[LPS/PBS]
H2-D1 0.59 -0.54
H2-K1 0.36 -0.98
H2-DMa 0.28 -0.54
H2-DMb1 0.29 -0.23
H2-DMb2 -0.01 -0.51
B2m 0.34 -0.76
Tap1 0.61 -0.01
Tapbp 0.02 -0.32
Ifit1 1.31 0.19
Ifit3 0.64 -0.60
Mx1 1.05 -0.29
Mx2 0.73 -0.10
Oas1a 1.85 0.18
Oas1g 1.29 -0.10
Isg15 1.32 -0.26
Irf7 1.76 0.43
Irf9 0.69 0.43

Figure 4

Figure 4. GWI Microglia mount a blunted transcriptional response to systemic LPS — the microglial-exhaustion phenotype.

(**a, b**) PCA and volcano plots for the comparative analysis for GWI effects under (**a**) basal (PBS) and (**b**) immune-stimulated (LPS) conditions (n = 3-4 per group). (**c**) Basal GWI microglia signature: pre-ranked GSEA-GO:BP showing elevated translation at synapse, ribosome, and oxidative phosphorylation categories in GWI microglia at baseline. (**d**) Number of GO:BP terms significantly enriched in DEGs from over-representation analysis (ORA) comparing LPS- versus PBS-treated GWI and control mice across a range of statistical stringencies. (**e**) Microglial cell-type module score panel across the four experimental groups: in control mice, LPS drives the canonical decrease in Homeostatic and increases in Complement, Interferon_Antiviral, and Phagocytosis_Lysosome modules, whereas in GWI none of these reach significance and Antigen_Presentation and Lipid_DAM modules respond to LPS in the opposite direction. (**f, g**) Immune-stimulated GWI microglia signature: pre-ranked GSEA-GO:BP showing reduced proton motive force-driven ATP synthesis, mitochondrial translation, ATP biosynthetic process, and oxidative phosphorylation (**f**), with leading-edge gene panels and corresponding $\log_2$[GWI/Ctrl] values in (**g**). (**h, i**) Pre-ranked GSEA summary of the formal GWI × LPS interaction (ΔLPS) within microglia, revealing reduced ribosome, oxidative phosphorylation, and translation at synapse pathways in GWI microglia (**h**) and leading-edge genes spanning ribosomal proteins, MHC molecules, and interferon-stimulated genes (**i**).

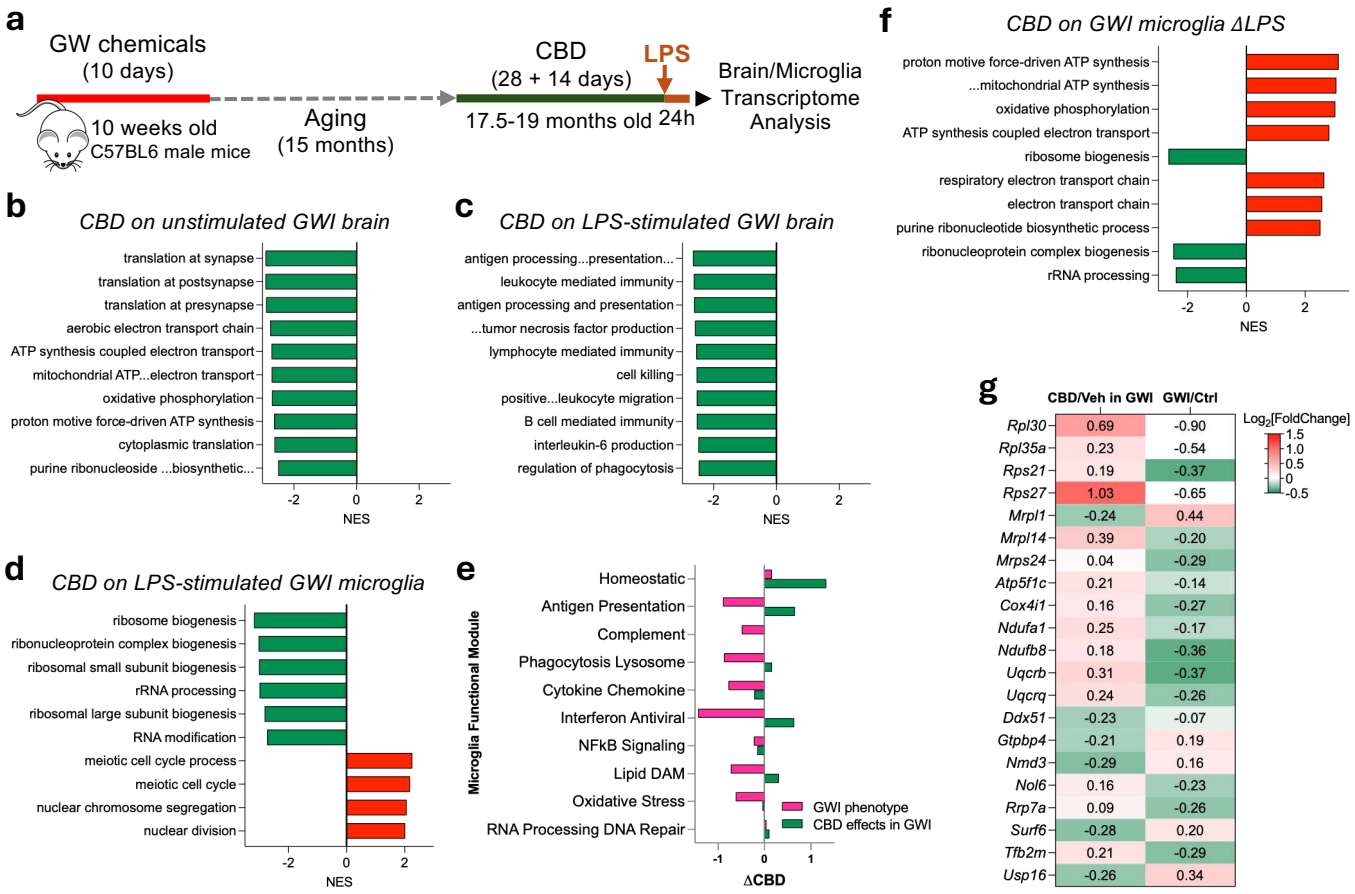

Figure 5. Chronic CBD partially rescues both arms of the GWI dual phenotype.
(**a**) Schematic of the CBD treatment paradigm: daily intraperitoneal CBD or vehicle for 28 days beginning 15 months after the GW chemicals exposure, followed by a single intraperitoneal LPS or PBS injection and tissue collection for bulk RNA-seq analysis of whole-brain and FACS-purified microglia. (**b**) Pre-ranked GSEA-GO:BP pathways down-regulated in whole brain by CBD, including translation at synapse and oxidative phosphorylation. (**c**) Top GSEA-GO:BP categories down-regulated in whole brain by CBD under LPS, led by antigen processing and presentation, leukocyte-mediated immunity, and lymphocyte/adaptive immunity. (**d**) GSEA-GO:BP results in LPS-stimulated microglia showing CBD-induced elevation of meiotic cell cycle program and reduction of ribosome biogenesis genes. (**e**) Functional module analysis indicating CBD-provided rescue of Antigen_Presentation and Interferon_Antiviral signatures in LPS-stimulated GWI microglia. (**f**) Formal CBD × LPS interaction in microglia revealing increased ATP synthesis, oxidative phosphorylation, and ribosome pathways driven by *Rpl/Rps/Mrpl/Mrps* gene families (**g**), alongside concurrent down-regulation of GO:BP ribosome biogenesis terms (**f**) driven by upstream regulators (**g**).

Figure 5

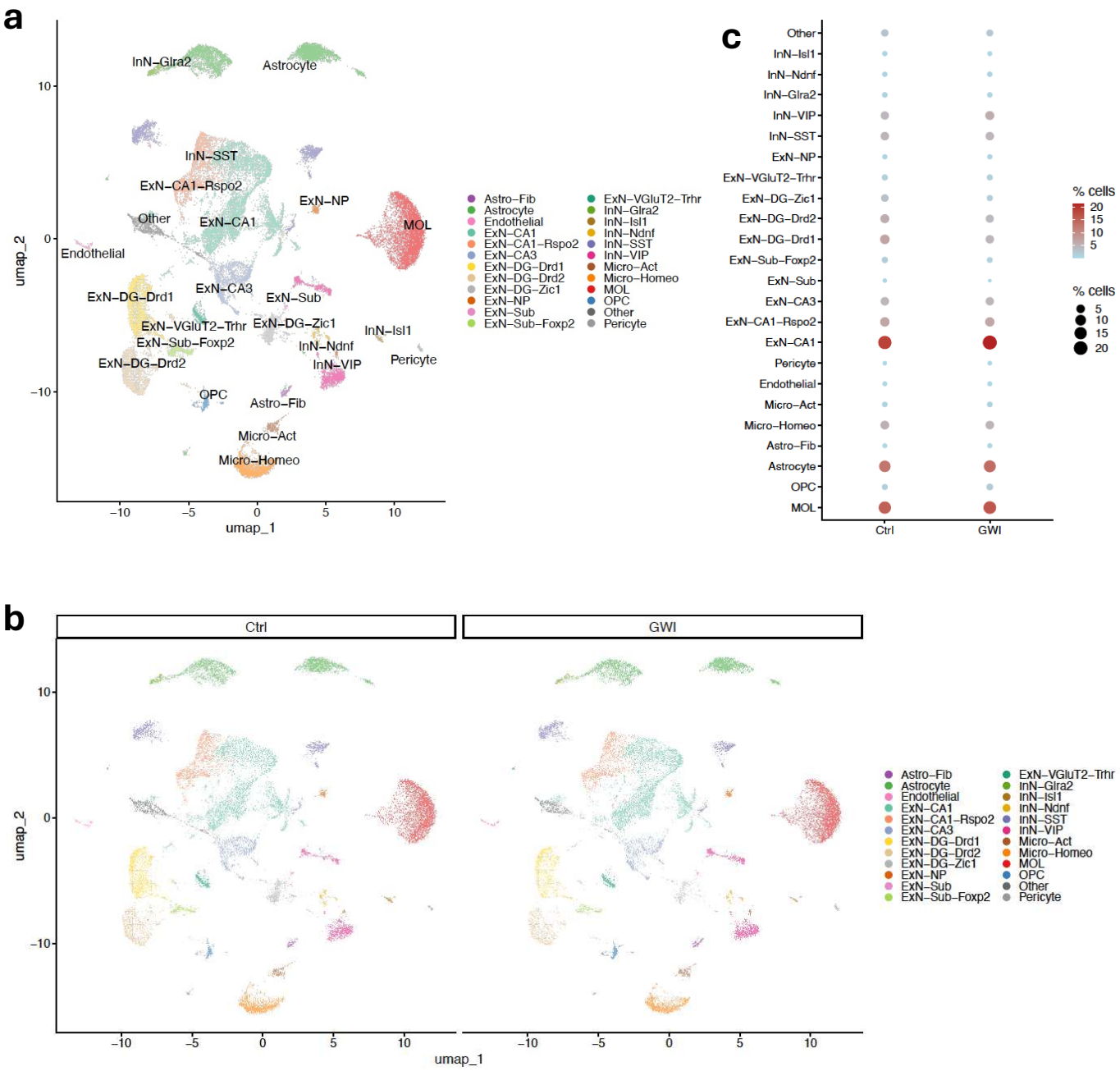

Supplementary Figure S1. Fine cell-type annotation of the hippocampal snRNA-seq atlas. (**a**) UMAP of 37,745 high-quality nuclei, Harmony-integrated and colored by 24 fine cell-type clusters. (**b**) UMAP split by condition (Ctrl, GWI). (**c**) Dot plot of canonical lineage markers.

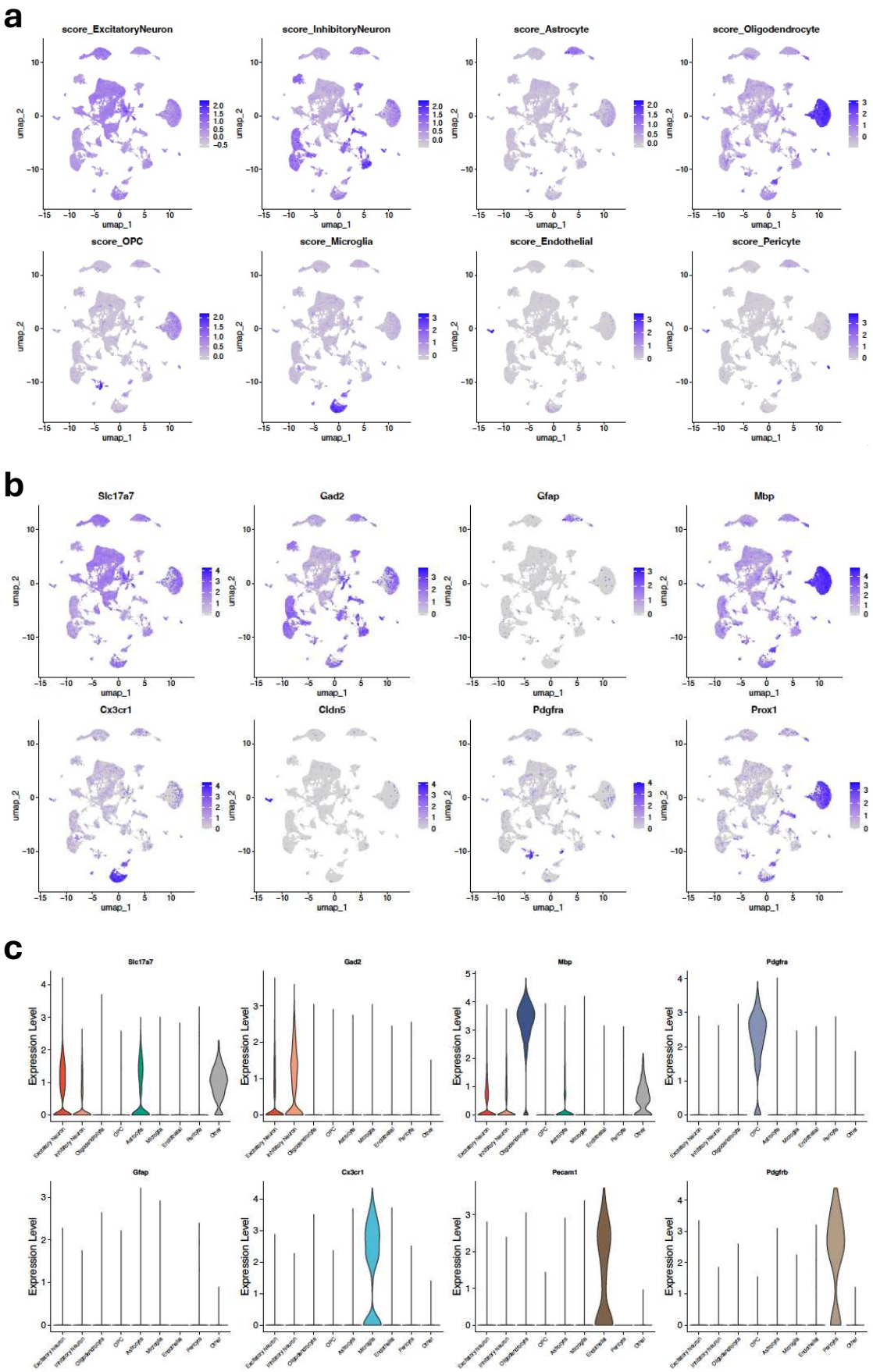

Supplementary Figure S2. Expression of canonical lineage markers. (**a**) Composite marker score UMAP. (**b**) UMAPs for individual cell-type markers. (**c**) Violin plots for the same markers across fine cell-type clusters.

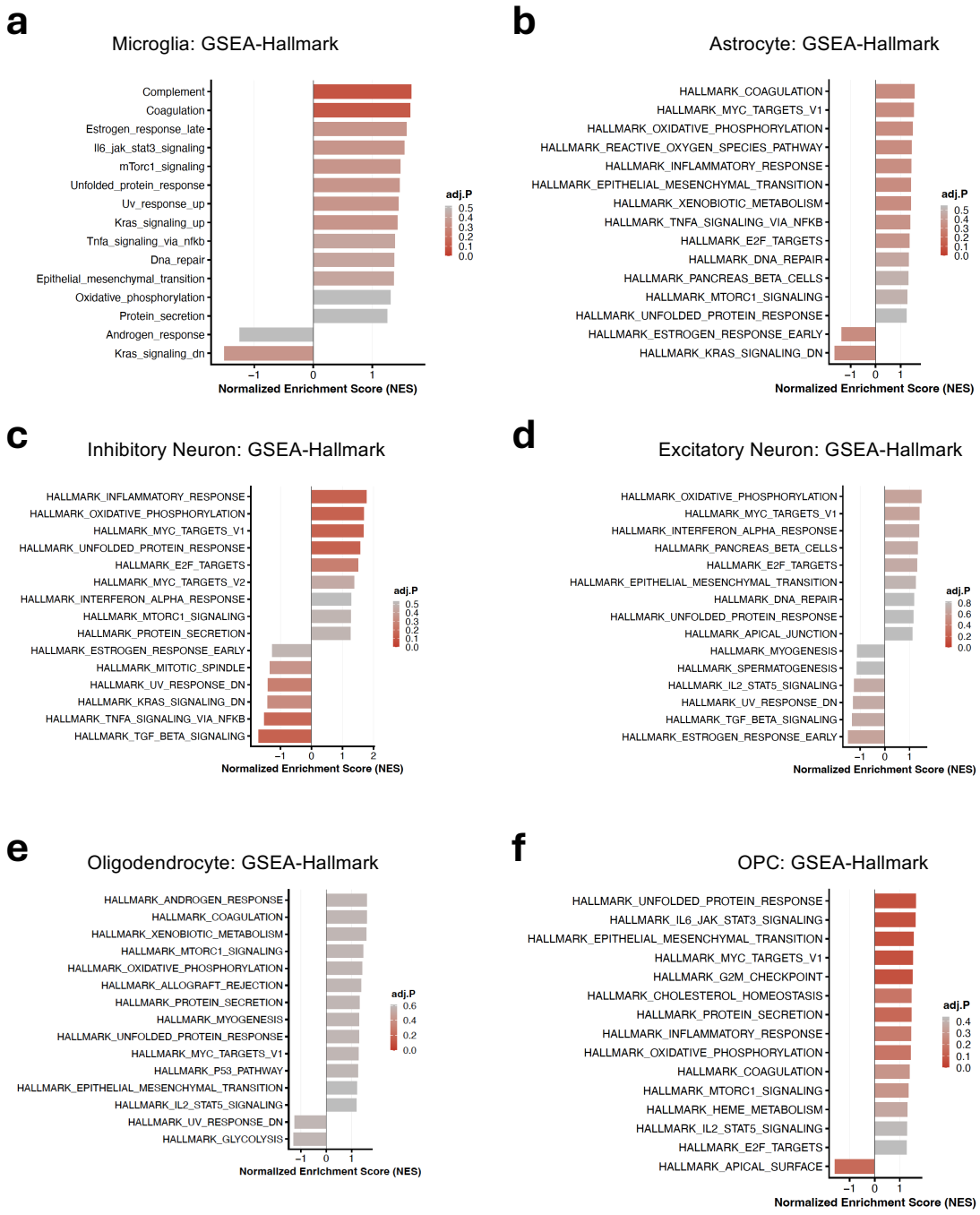

Supplementary Figure S3. Hallmark pathway enrichment in broad cell-type clusters. GSEA-Hallmark panels for broadly annotated hippocampal cell type clusters: (**a**) microglia, (**b**) astrocyte, (**c**) inhibitory neurons, (**d**) excitatory neurons, (**e**) oligodendrocyte, and (**f**) OPC.

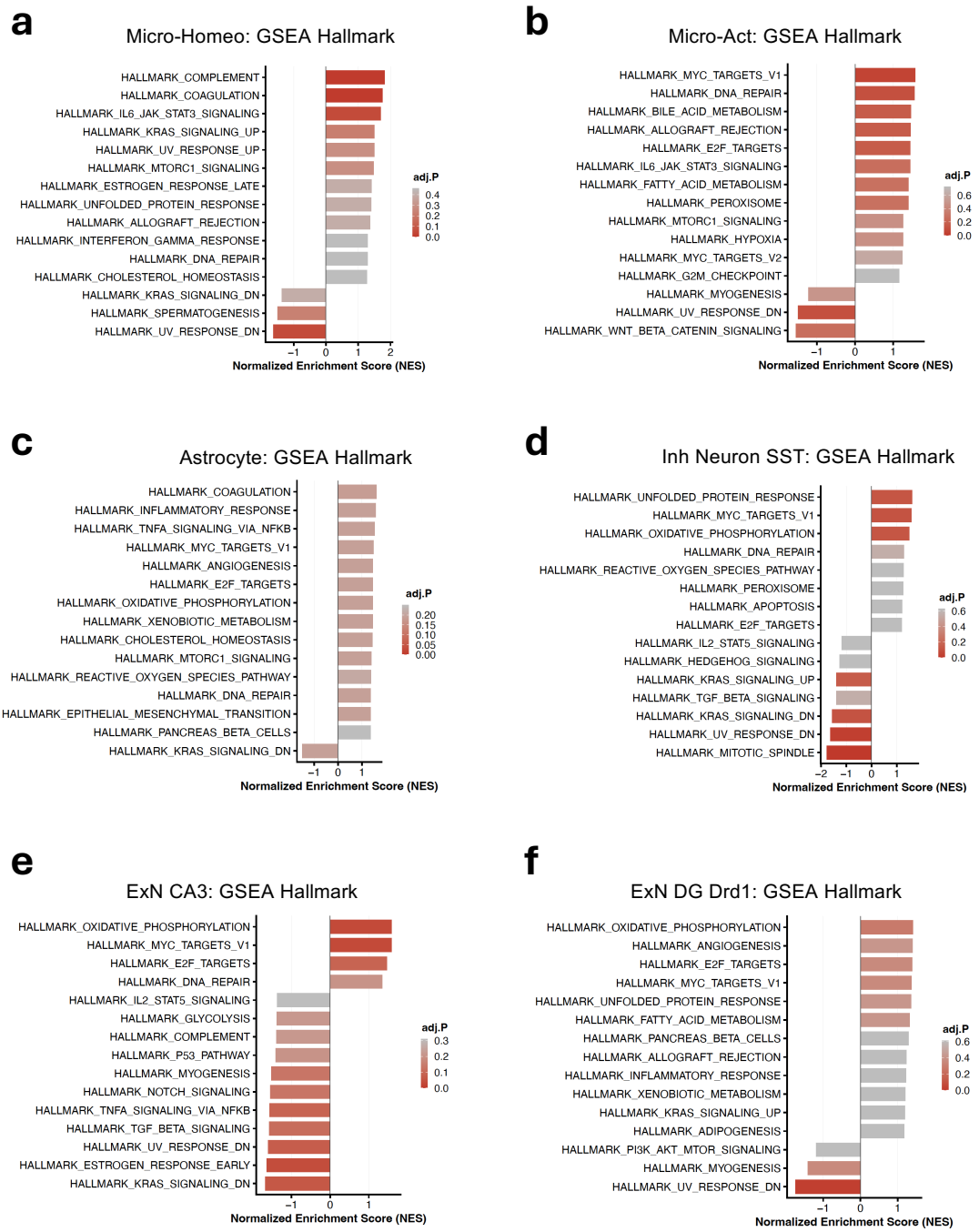

Supplementary Figure S4. Hallmark pathway enrichment in selected fine cell-type clusters. GSEA-Hallmark panels for selected fine cell type annotation clusters: (**a**) homeostatic microglia (Micro-Homeo), (**b**) activated microglia (Micro-Act), (**c**) astrocyte, (**d**) SST-expressing inhibitory neurons (**e**) CA3 excitatory neurons, and (**f**) Drd1-expressing excitatory neurons in DG.

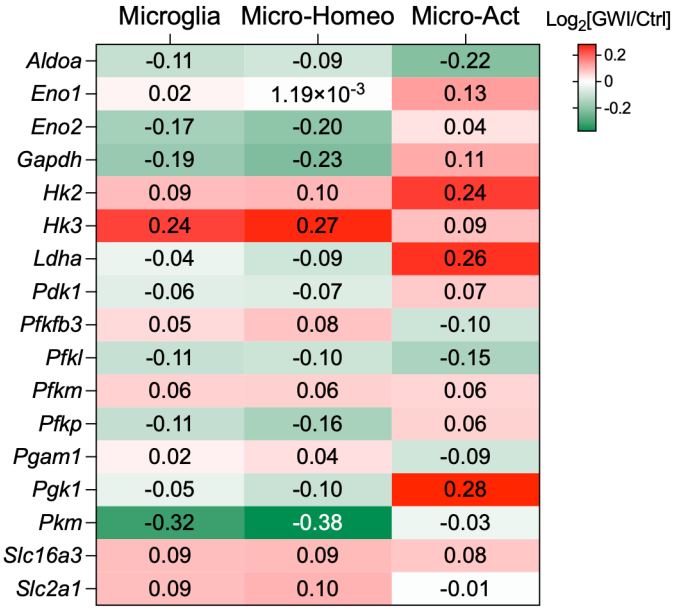

Supplementary Figure S5. Glycolytic gene expression across microglia clusters. Heatmap for glycolytic gene expression across the broad microglial cluster and its fine subsets, including activated microglia (Micro-Act) and homeostatic microglia (Homeo-Act); values indicate the $\log_2$[GWI/Ctrl] for each gene.

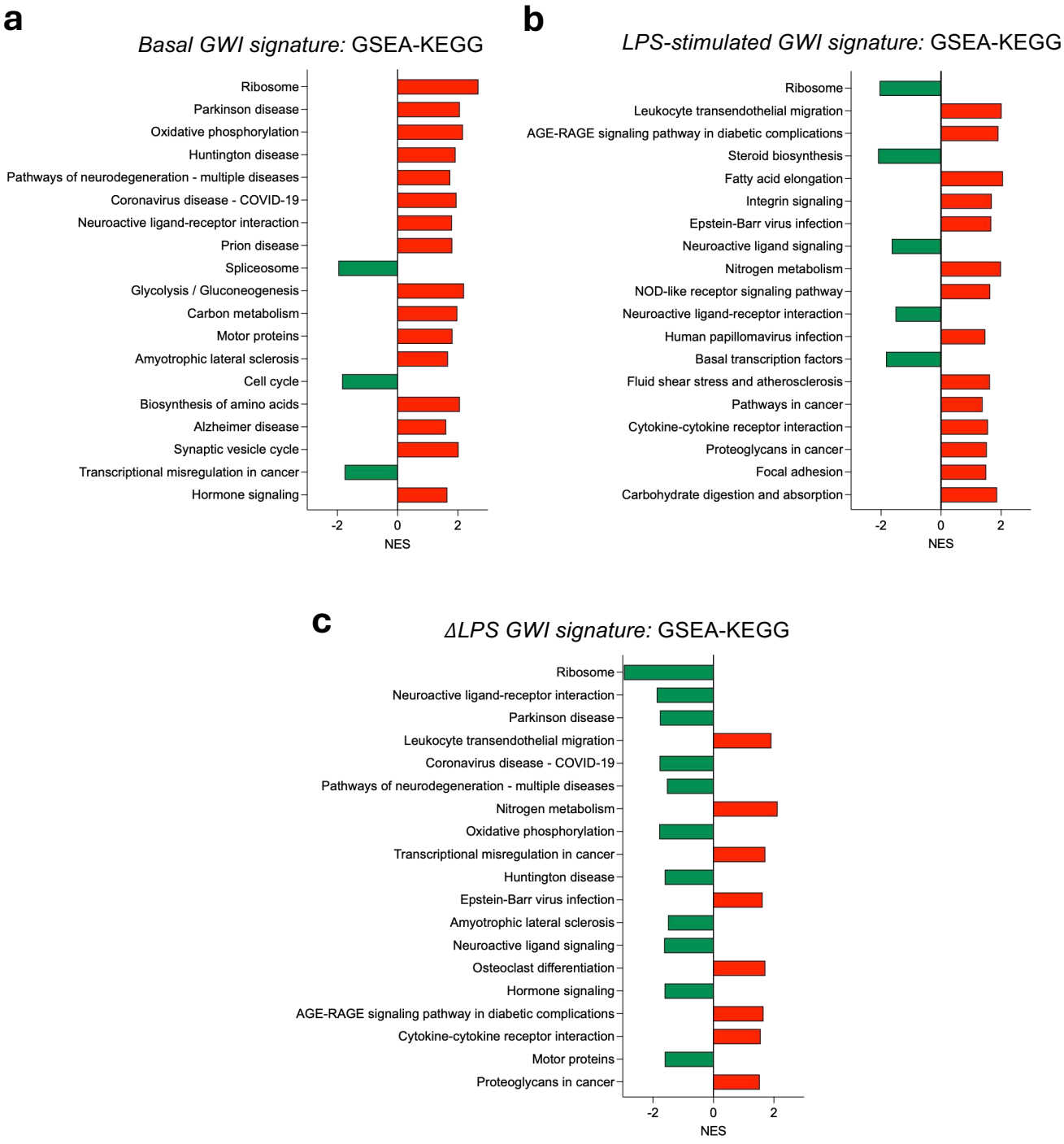

Supplementary Figure S6. Whole-brain bulk RNA-seq GSEA-KEGG enrichment for GWI. Whole-brain bulk RNA-seq GSEA-KEGG results for the effects of GWI versus control under basal unstimulated conditions (**a**), LPS-stimulated conditions (**b**), and the formal GWI × LPS interaction (ΔLPS) (**c**).

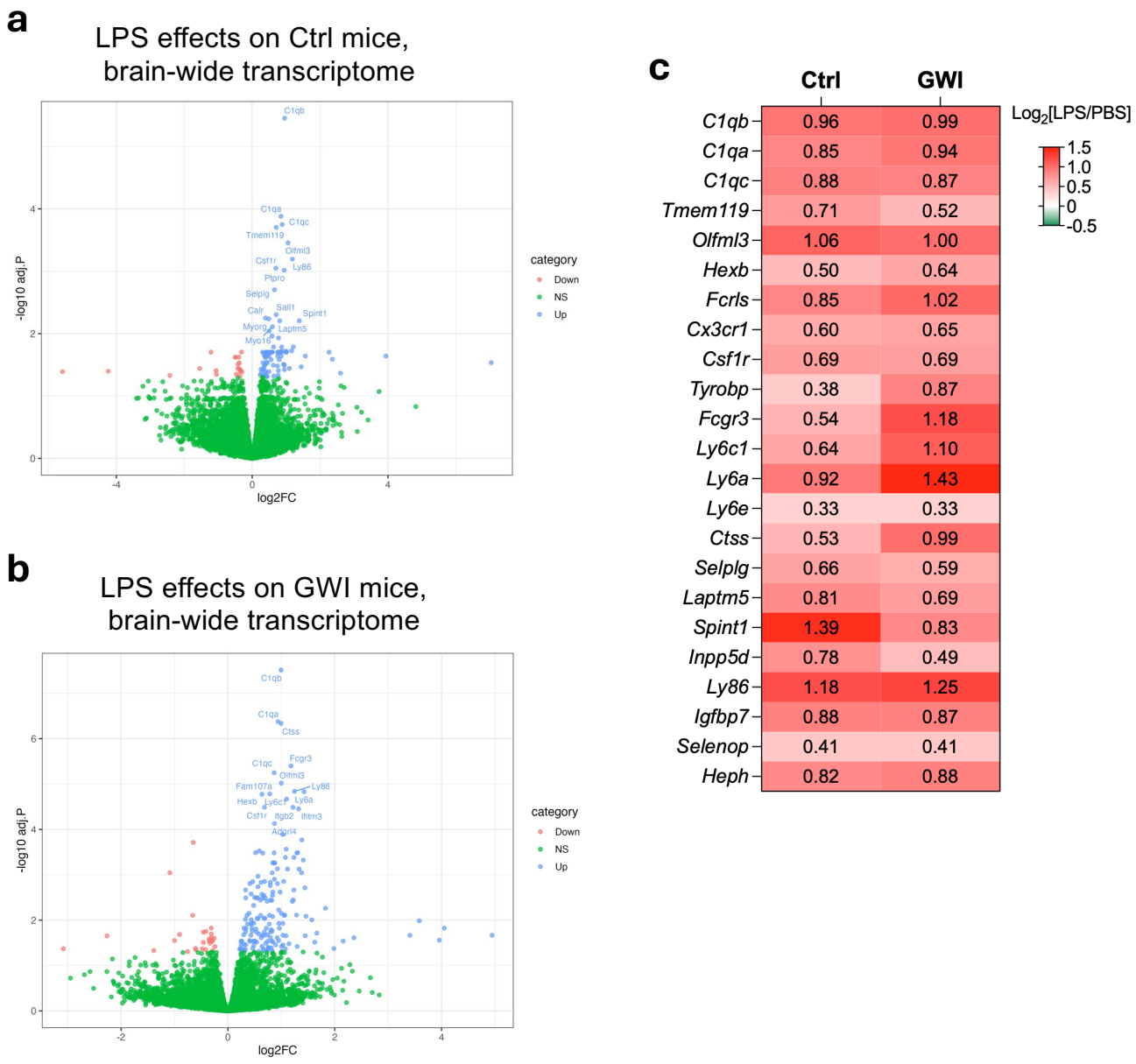

Supplementary Figure S7. Brain-wide response to LPS stimulation in aged control and GWI mice. (**a, b**) Volcano plots for LPS versus PBS in (**a**) Ctrl and (**b**) GWI mice. (**c**) Heatmap showing LPS-induced transcriptional changes in select neuroinflammation-related genes in control and GWI mice; numbers indicate $\log_2$[LPS/PBS] for each gene.

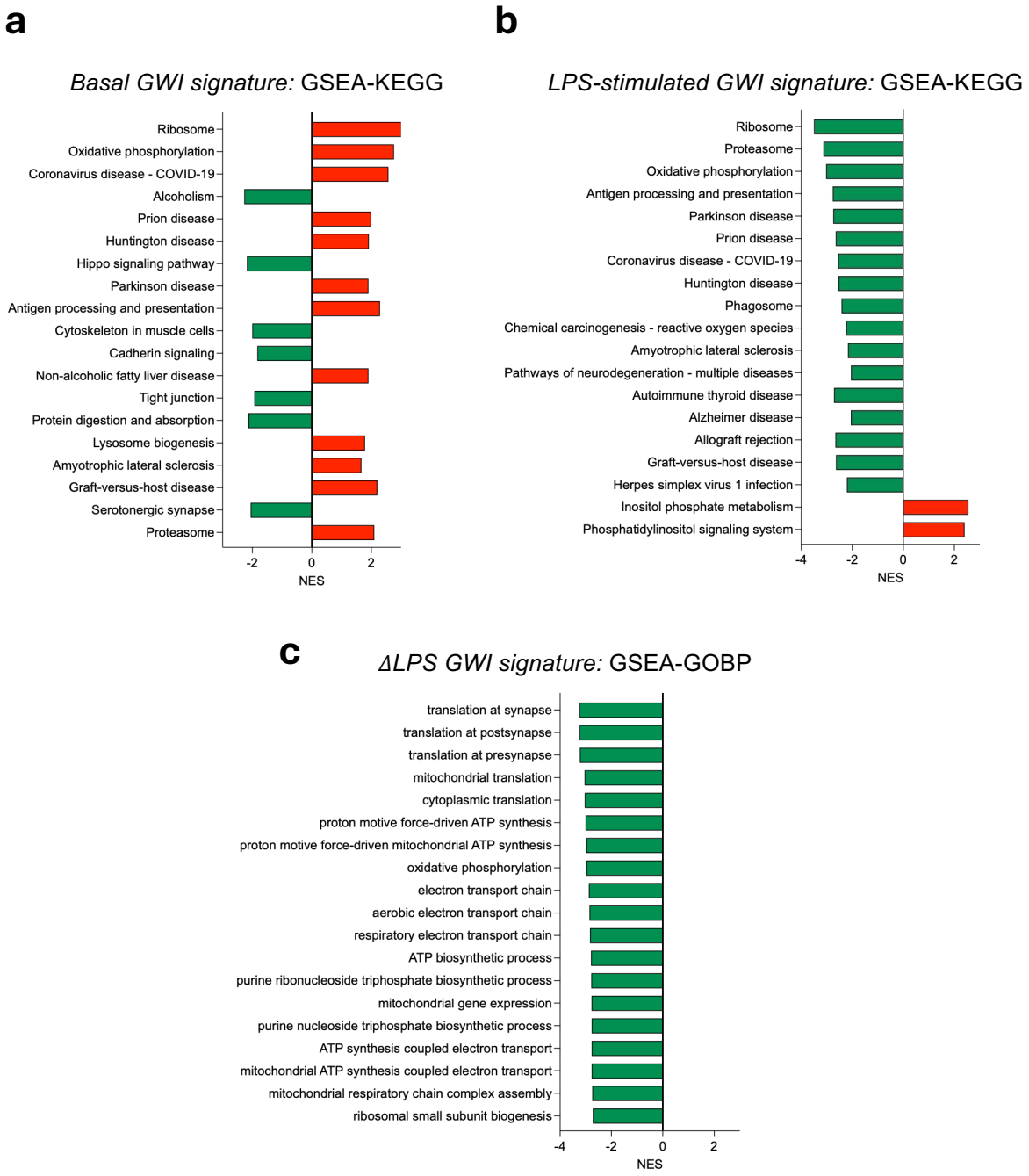

Supplementary Figure S8. Microglia bulk RNA-seq GSEA-KEGG and GSEA-GO:BP enrichment for GWI. Microglia bulk RNA-seq GSEA results for the effects of GWI versus control under basal, unstimulated conditions (**a,** GSEA-KEGG), LPS-stimulated conditions (**b,** GSEA-KEGG), and the formal GWI × LPS interaction (ΔLPS) (**c,** GSEA-GO:BP).

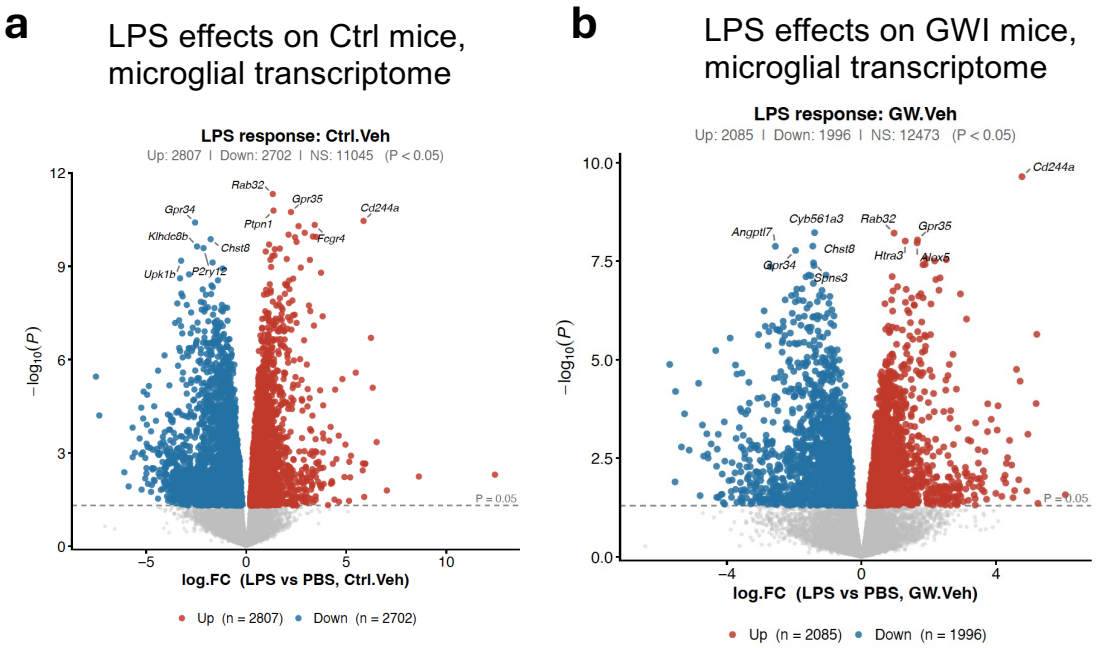

Supplementary Figure S9. Microglial response to LPS stimulation in aged control and GWI mice. Volcano plots for LPS versus PBS in microglia from (**a**) Ctrl and (**b**) GWI mice.

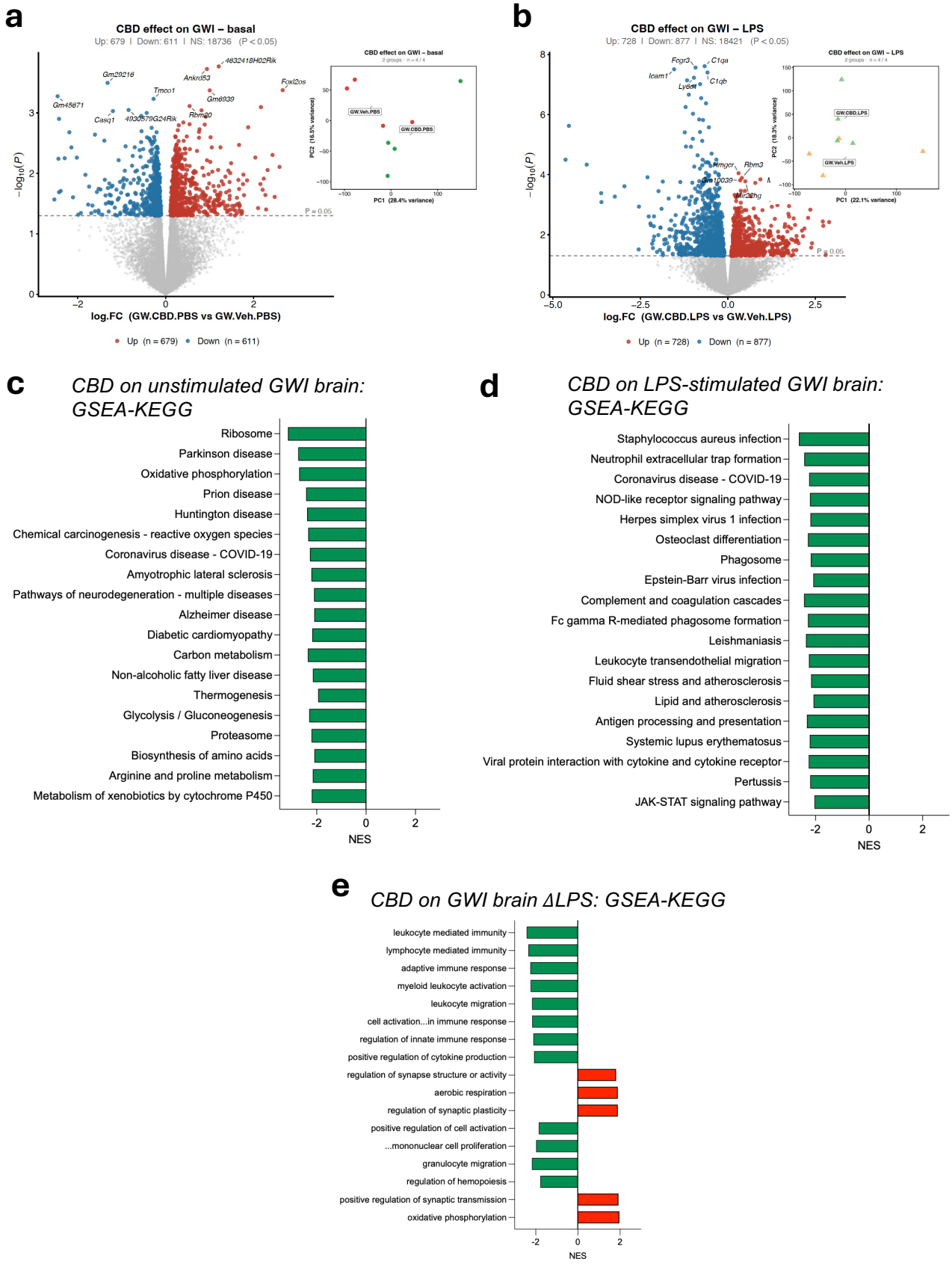

Supplementary Figure S10. Brain-wide response to CBD treatment in aged GWI mice. (**a, b**) PCA and volcano plots for CBD versus vehicle treatment in GWI mice under (**a**) basal, unstimulated and (**b**) LPS-stimulated conditions. (**c, d**) Whole-brain bulk RNA-seq GSEA-KEGG results for CBD versus vehicle in GWI mice under basal (**c**) and LPS-stimulated (**d**) conditions. (**e**) GSEA-KEGG results for the formal GWI × LPS interaction (ΔLPS).

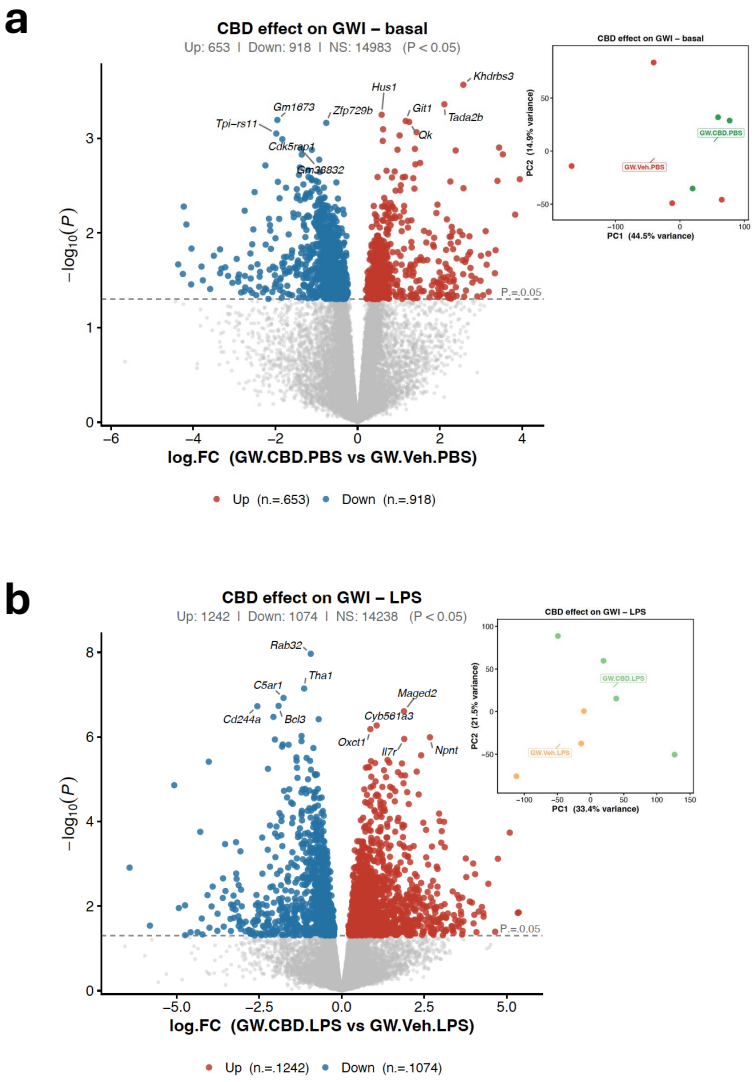

Supplementary Figure S11. Microglial response to CBD treatment in aged GWI mice. (**a, b**) PCA and volcano plots for CBD versus vehicle in microglia from GWI mice under (**a**) basal, unstimulated and (**b**) LPS-stimulated conditions.

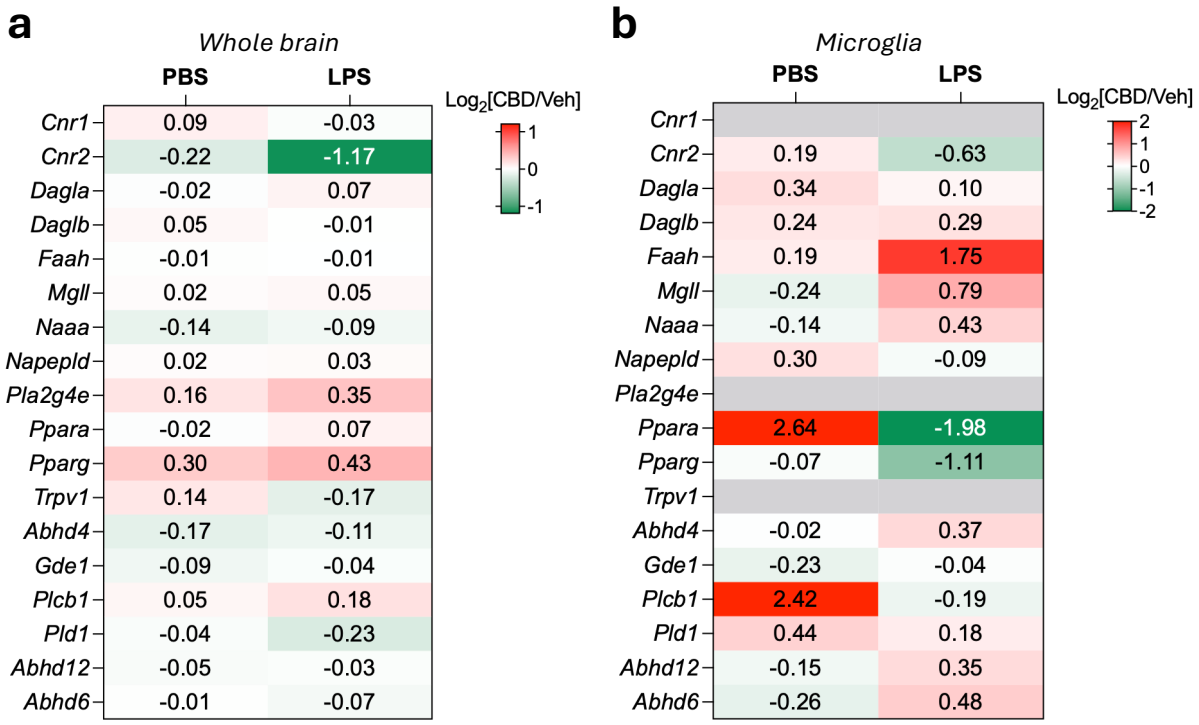

Supplementary Figure S12. Effects of CBD treatment on endocannabinoid (ECB)-related genes in GWI mice. Heatmap showing CBD-induced transcriptional changes in select ECB system genes in the (**a**) whole brain or (**b**) purified microglia from GWI mice, under unstimulated (PBS) or LPS-stimulated conditions; numbers indicate $\log_2$[CBD/Veh] for each gene.

Supplementary Files

This is a list of supplementary files associated with this preprint. Click to download.

- TableS1SummarysnRNAseqcellannotation.xlsx
- TableS5BrainwideLPSEffectsUpDEGGOBP.xlsx
- TableS6BrainwidedeltaLPSGSEAGOBPKEGG.xlsx
- TableS12ListCelltypeModuleGenes.xlsx
- TableS8MicrogliaLPSEffectsUpDEGGOBP.xlsx
- TableS3Globalmoduleanalysis.xlsx
- TableS4BrainwideDEGGOKEGGsummarycounts.xlsx
- TableS7MicrogliaDEGGOKEGGsummarycounts.xlsx
- TableS11MicrogliaCBDEffectsGWILPSGSEAGOBPKEGG.xlsx
- TableS2SummaryGSEAsnRNAseqCellType.xlsx
- TableS9BrainwideCBDEffectsDownDEGGWILPSGOBP.xlsx
- TableS10MicrogliaCBDEffectsDownUpDEGGWILPSGOBP.xlsx